

$\bar{K} + N \rightarrow K + \Xi$ reaction and $S = -1$ hyperon resonances

Benjamin C. Jackson,¹ Yongseok Oh,^{2,3,*} H. Haberzettl,^{4,†} and K. Nakayama^{1,5,‡}

¹*Department of Physics and Astronomy, The University of Georgia, Athens, GA 30602, USA*

²*Department of Physics, Kyungpook National University, Daegu 702-701, Korea*

³*Asia Pacific Center for Theoretical Physics, Pohang, Gyeongbuk 790-784, Korea*

⁴*Institute for Nuclear Studies and Department of Physics,
The George Washington University, Washington, DC 20052, USA*

⁵*Institut für Kernphysik and Center for Hadron Physics,
Forschungszentrum Jülich, 52425 Jülich, Germany*

(Dated:)

The $\bar{K}N \rightarrow K\Xi$ reaction is studied based on an effective Lagrangian approach that includes the hyperon s - and u -channel contributions as well as the phenomenological contact amplitude. The latter accounts for the rescattering term in the scattering equation and the possible short-range dynamics not included explicitly in the model. Existing data is well reproduced and three above-threshold resonances were found to be required to describe the data, namely, the $\Lambda(1890)$, $\Sigma(2030)$, and $\Sigma(2250)$. For the latter resonance we have assumed the spin-parity of $J^P = 5/2^-$ and a mass of 2265 MeV. The $\Sigma(2030)$ resonance is critical to achieve a good reproduction of not only the measured total and differential cross sections, but also the recoil polarization asymmetry. More precise data are required before a more definitive statement can be made about the other two resonances, in particular, about the $\Sigma(2250)$ resonance that is introduced to describe a small bump structure observed in the total cross section of $K^-p \rightarrow K^+\Xi^-$. Predictions for the target-recoil asymmetries of the $\bar{K}N \rightarrow K\Xi$ reaction are also presented.

PACS numbers: 13.75.Jz, 13.60.Rj, 13.88.+e, 14.20.Jn

I. INTRODUCTION

Hadron spectroscopy is an essential part of the investigation to understand the non-perturbative regime of Quantum Chromodynamics (QCD). In principle, an ab-initio approach to hadron resonance physics can be provided by lattice QCD simulation. In particular, the spectra of excited baryons observed in the recent lattice simulations [1, 2] hold the promise of explaining the rich dynamics in the resonance energy region in the near future. Once quark masses drop towards the physical limit and finite volume effects are fully under control, a close comparison to experimental data will be possible. Other approaches such as the dynamical Dyson-Schwinger [3], constituent quark models [4, 5], and the Skyrme model [6] also generate resonance spectra. Unitarized Chiral Perturbation Theory also provides a complementary picture of some of the low-lying resonances [7, 8]. To compare these theoretical results with the experimental data, a reliable reaction theory capable of identifying resonances and extracting the corresponding resonance parameters is required. Such reaction theories, based on a coupled-channel approach, have been developed at various degree of sophistication and are being improved [9–16]. So far, most of the experimentally extracted baryon resonances come from the pion-induced reaction experiments, especially the πN scattering, and about 16 nucleon resonances and 11 Δ resonances have been identified [17].

A number of Λ and Σ baryons, which are particles with strangeness quantum number $S = -1$, have been also discovered [17]. A review on the status of baryon spectroscopy is given, e.g., in Ref. [18].

Although the multi-strangeness baryons ($S < -1$) have played an important role in the development of our understanding of strong interactions, and thus, should be an integral part of any baryon spectroscopy program, the current knowledge of these baryons is still extremely limited. In fact, the SU(3) flavor symmetry allows as many $S = -2$ baryon resonances, called Ξ , as there are N and Δ resonances combined (~ 27); however, until now, only eleven Ξ baryons have been discovered [17]. Among them, only three [ground state $\Xi(1318)1/2^+$, $\Xi(1538)3/2^+$, and $\Xi(1820)3/2^-$] have their quantum numbers assigned.¹ This situation is mainly due to the fact that multi-strangeness particle productions have relatively low yields. For example, if there are no strange particles in the initial state, Ξ is produced only indirectly and the yield is only of the order of nb in the photoproduction reaction [19], whereas the yield is of the order of μb [20] in the hadronic, \bar{K} -induced reaction, where the Ξ is produced directly because of the presence of an $S = -1$ \bar{K} meson in the initial state. The production rates for Ω baryons with $S = -3$ are even much lower [21].

The study of multi-strangeness baryons has started to attract a renewed interest recently. Indeed, the CLAS

* yohphy@knu.ac.kr

† helmut@gwu.edu

‡ nakayama@uga.edu

¹ The parity of the ground state Ξ has not been measured explicitly yet, but its assignment is based on quark models and SU(3) flavor symmetry.

Collaboration at Thomas Jefferson National Accelerator Facility (JLab) plans to initiate a Ξ spectroscopy program using the upgraded 12-GeV machine, and measure the exclusive Ω photoproduction for the first time [22]. Some data for the production of the Ξ ground state, obtained from the 6-GeV machine, are already available [19]. They were analyzed by some of the present authors [23, 24] within an effective Lagrangian approach. J-PARC is going to study the Ξ baryons via the $\bar{K}N \rightarrow K\Xi$ process (which is the reaction of choice for producing Ξ) in connection to its program proposal for obtaining information on Ξ hypernuclei spectroscopy. It also plans to study the $\pi N \rightarrow KK\Xi$ reaction as well as Ω production [25, 26]. At the FAIR facility of GSI, the reaction $\bar{p}p \rightarrow \Xi\Xi$ will be studied by the PANDA Collaboration [27]. Quite recently, also lattice QCD calculations of the baryon spectra, including those of Ξ and Ω baryons, have been reported, for example, in Refs. [1, 2].

In the present work we concentrate on the production of $S = -2$ Ξ , in particular, on the production reaction process of the ground state Ξ ,

$$\bar{K}(q) + N(p) \rightarrow K(q') + \Xi(p'). \quad (1)$$

This reaction has been studied experimentally, mainly, throughout the 60's [28–37], which was followed by several measurements made in the 70's and 80's [38–44]. The existing data are rather limited and suffer from large uncertainties. The total cross section and some of the differential cross section data are tabulated in Ref. [20]. We shall return to the discussion of these experimental data later on. Early theoretical attempts to understand the above reaction are very few and can be found in Refs. [45–49]. To date, recent calculations are reported by Sharov *et al.* [50] and by Shyam *et al.* [51]. The former authors have considered both the total and differential cross sections as well as the recoil polarization data in their analysis, while the latter authors have considered only the total cross section data, although they too have predicted the differential cross sections, mentioning that they found it difficult to use the differential cross section data [37] for several reasons. Although the analyses of Refs. [50, 51] are both based on very similar effective Lagrangian approaches, the number of $S = -1$ hyperon resonances included in the intermediate state are different. While in Ref. [50] only the $\Sigma(1385)$ and $\Lambda(1520)$ are considered in addition to the above-threshold $\Sigma(2030)$ and $\Sigma(2250)$ resonances,² in Ref. [51] eight of the 3- and 4-star Λ and Σ resonances with masses up to 2.0 GeV have been considered. While the authors of Ref. [50] pointed out the significance of the above-threshold resonances, the authors of Ref. [51] have found the dominance of the sub-threshold $\Lambda(1520)$ resonance. The reaction (1) has been also considered quite recently by Magas *et al.* [52]

within the coupled channels Unitarized Chiral Perturbation approach in connection to the issue of determining the parameters of the next-to-leading-order interactions. The authors of Ref. [52] have added the $\Sigma(2030)$ and $\Sigma(2250)$ resonances into their calculation to improve the fit quality to the total cross section data. Just recently, a calculation by the Argonne-Osaka group [53] within a Dynamical Coupled Channels approach to the \bar{K} -induced two-body reactions up to $W = 2.1$ GeV has been also reported. There too, only the total cross sections were considered.

On the other hand, some of the model-independent aspects of the reaction (1) have been studied recently by the present authors [54, 55]. In the present work, we perform a model-dependent analysis of the existing data based on the effective Lagrangian approach that includes a phenomenological contact amplitude which accounts for the rescattering contributions and/or unknown (short-range) dynamics that have not been included explicitly into the model.

It should be mentioned that the present study is our first step toward building a more complete reaction model capable of extracting reliably the properties of hyperons from the forthcoming experimental data, in addition to providing some guidance for planning future experiments. The investigation of the reaction (1) impacts also the study of Ξ hypernuclei, where the elementary process of Eq. (1) is an input to the models of hypernuclei productions [49, 56–58]. As mentioned before, there is a proposed program at J-PARC and eventually at GSI-FAIR to obtain information about the spectroscopy of Ξ hypernuclei through the anti-kaon induced reactions on nuclear targets. Establishing the existence and properties of Ξ hypernuclei is of considerable importance for a number of reasons and the study of the reaction (1) is an essential step to this end.

The present paper is organized as follows. In Sec. II, our model for describing the reaction of Eq. (1) is presented. Some details of the model are given in the Appendix. In Sec. III, the results of our model calculations are presented and discussed. Section IV summarizes our conclusions.

II. MODEL DESCRIPTION

The reaction amplitude T describing the two-body process like the reaction (1) is, in general, given by the Bethe-Salpeter equation,

$$T = V + VGT, \quad (2)$$

where V stands for the (two-body) meson-baryon irreducible (Hermitian) driving amplitude and G the meson-baryon propagator. Note that the above equation represents, in principle, a coupled-channels equation in meson-baryon channel space. It can be recast into the pole and the non-pole parts as

$$T = T^P + T^{\text{NP}}, \quad (3)$$

² The production threshold energy for the reaction of Eq. (1) is about 1813 MeV.

where the non-pole part T^{NP} obeys

$$T^{\text{NP}} = V^{\text{NP}} + V^{\text{NP}} G T^{\text{NP}} \quad (4)$$

with

$$V^{\text{NP}} \equiv V - V^{\text{P}} \quad (5)$$

denoting the one-baryon irreducible (non-pole) part of the driving amplitude V . Here, V^{P} stands for the one-baryon reducible (pole) part of V in the form of

$$V^{\text{P}} = \sum_r |F_{0r}\rangle S_{0r} \langle F_{0r}|, \quad (6)$$

where $|F_{0r}\rangle$ and $S_{0r} = (p_r^2 - m_{0r}^2 + i\eta)^{-1}$ stand for the so-called bare vertex and bare baryon propagator, respectively. The summation runs over the baryons in the intermediate state, each specified by the index r . The four-momentum and the bare mass of the propagating baryon are denoted by p_r and m_{0r} , respectively. It can be understood that V^{P} is nothing other than the sum of the s -channel Feynman diagrams corresponding to the bare baryon propagations in the intermediate state as can be seen in Fig. 1. The pole part of the reaction amplitude T^{P} in Eq. (3) is given by

$$T^{\text{P}} = \sum_{r'r} |F_{r'}\rangle S_{r'r} \langle F_r|, \quad (7)$$

where the so-called dressed vertex reads

$$\begin{aligned} |F_{r'}\rangle &= (1 + T^{\text{NP}} G) |F_{0r'}\rangle, \\ \langle F_r| &= \langle F_{0r}| (1 + G T^{\text{NP}}), \end{aligned} \quad (8)$$

and the dressed propagator $S_{r'r}$ is written as

$$S_{r'r}^{-1} = S_{0r}^{-1} \delta_{r'r} - \Sigma_{r'r}, \quad (9)$$

with

$$\Sigma_{r'r} = \langle F_{0r'} | G | F_r \rangle \quad (10)$$

denoting the self-energy.

In the present work we shall make the following approximations to the reaction amplitude in Eq. (3). First, we approximate the pole part of the reaction amplitude T^{P} by the s -channel Feynman amplitude, M_s , specified by effective Lagrangians and phenomenological Feynman propagators. Here, the dressed resonance coupling constants, dressed masses as well as the corresponding widths are parameters either fixed from independent sources or adjusted to reproduce the experimental data. The couplings of the resonances in the propagator are ignored in the present work. More explicitly, we have

$$\begin{aligned} |F_{r'}\rangle &\rightarrow \hat{\Gamma}_{MBr'}^\dagger, \\ \langle F_r| &\rightarrow \hat{\Gamma}_{MBr}, \\ S_{r'r} &\rightarrow \hat{S}_r \delta_{r'r}, \end{aligned} \quad (11)$$

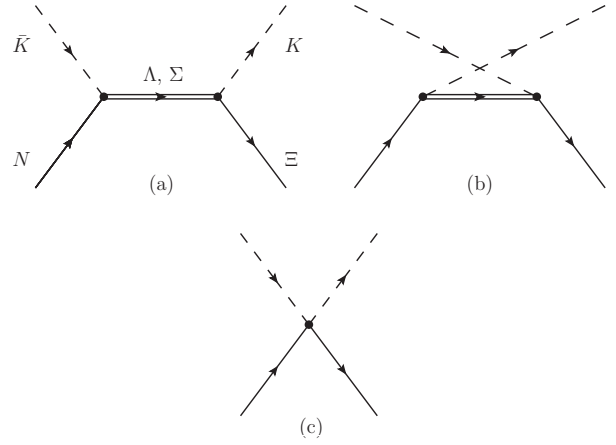


FIG. 1. Diagrams included in the present calculation. (a) s -channel Λ and Σ hyperon exchange amplitude, M_s . (b) u -channel amplitude, M_u , including the same hyperon exchanges as in (a). (c) contact amplitude, M_c , as discussed in Sec. II.

with the subscripts M and B denoting a meson and a baryon, respectively. The meson-baryon-baryon vertices of $MB \rightarrow r'$ and $r \rightarrow MB$ are denoted by $\Gamma_{MBr'}^\dagger$ and Γ_{MBr} , respectively, and can be obtained from the effective Lagrangians given in the Appendix. The phenomenological Feynman propagators for dressed baryon \hat{S}_r are also given in the Appendix.

Second, the non-pole part of the reaction amplitude T^{NP} is approximated as follows.

- (i) Since there is no meson-exchange t -channel process in the present reaction unless the exchanged meson is an exotic one with strangeness quantum number $S = 2$, V^{NP} of the reaction is approximated by the u -channel Feynman amplitude M_u constructed also from the same effective Lagrangians and Feynman propagators used to construct the s -channel Feynman amplitudes.
- (ii) The rescattering term $V^{\text{NP}} G T^{\text{NP}}$ in T^{NP} of Eq. (4) and other effects not included explicitly in the present approach are accounted for by a phenomenological contact term, M_c , which is specified below. This contact term will be discussed in more detail later.

With the approximations described above, the reaction amplitude in the present work is given by

$$T = M_s + M_u + M_c, \quad (12)$$

where M_s and M_u are the s - and u -channel Feynman diagrams with the ground state hyperons as well as some of the $S = -1$ hyperon resonances in the intermediate state. Figure 1 shows a diagrammatic representation of M_s , M_u , and M_c .

The contact amplitude M_c is decomposed in terms of the spin-flip and spin-non-flip amplitudes, each expanded

in partial-waves. The spin amplitude for the reaction of Eq. (1) can be expanded in partial waves as³

$$\begin{aligned} M_{\frac{1}{2}, \frac{1}{2}} &= M_{-\frac{1}{2}, -\frac{1}{2}} \\ &= \frac{1}{4\pi} \sum_{LT} \left[(L+1) M_{LL}^{TJ+}(p', p) + L M_{LL}^{TJ-}(p', p) \right] \\ &\quad \times P_L(\hat{\mathbf{p}} \cdot \hat{\mathbf{p}}') \hat{P}_T, \end{aligned} \quad (13a)$$

$$\begin{aligned} M_{\frac{1}{2}, -\frac{1}{2}} &= -M_{-\frac{1}{2}, \frac{1}{2}} \\ &= \frac{1}{4\pi} \sum_{LT} \left[M_{LL}^{TJ-}(p', p) - M_{LL}^{TJ+}(p', p) \right] \\ &\quad \times P_L^1(\hat{\mathbf{p}} \cdot \hat{\mathbf{p}}') \hat{P}_T, \end{aligned} \quad (13b)$$

where the indices s' and (s) in $M_{s's}$ stands for the spin-projection quantum number of the final (initial) state and $J_{\pm} \equiv L \pm \frac{1}{2}$. The Legendre and associated Legendre functions are denoted by $P_L(x)$ and $P_L^1(x)$, respectively.⁴ The total angular momentum, orbital angular momentum, and total isospin of the initial $\bar{K}N$ state are represented by J, L , and T , respectively. \hat{P}_T stands for the isospin projection operator onto the total isospin 0 or 1 as $T = 0$ or $T = 1$, respectively. Explicitly, $\hat{P}_{T=0} = (3 + \boldsymbol{\tau}_1 \cdot \boldsymbol{\tau}_2)/4$ and $\hat{P}_{T=1} = (1 - \boldsymbol{\tau}_1 \cdot \boldsymbol{\tau}_2)/4$.

Following the essential idea of Ref. [59] for the phenomenological contact term, M_c , the spin amplitudes in the above equation corresponding to M_c are parametrized as

$$\begin{aligned} M_{c \frac{1}{2} \frac{1}{2}} &= M_{c -\frac{1}{2} -\frac{1}{2}} \\ &= \sum_{LT} g_1^{LT} \left(\frac{p'}{\Lambda_S} \right)^L \exp \left[-\alpha_L^T \frac{p'^2}{\Lambda_S^2} \right] P_L(\theta) \hat{P}_T, \\ M_{c \frac{1}{2} -\frac{1}{2}} &= -M_{c -\frac{1}{2} \frac{1}{2}} \\ &= \sum_{LT} g_2^{LT} \left(\frac{p'}{\Lambda_S} \right)^L \exp \left[-\beta_L^T \frac{p'^2}{\Lambda_S^2} \right] P_L^1(\theta) \hat{P}_T \end{aligned} \quad (14)$$

with $g_1^{LT} \equiv a_L^T \exp(i\{\phi_a\}_L^T)$, $g_2^{LT} \equiv b_L^T \exp(i\{\phi_b\}_L^T)$, and α_L^T, β_L^T being constants to be fitted. Λ_S is a typical scale parameter of the reaction at hand. The momentum dependence of the partial-wave matrix elements given above is suited for hard processes, where one has a large momentum transfer for, in those processes, the amplitude is expected to be independent of energy and nearly constant apart from the centrifugal barrier effect. The reaction (1) is not a very hard process.⁵ Nonetheless,

the p'^L -dependence captures the essence of the behavior of the amplitude at low momentum in the final state. We refer the details to Ref. [59]. The exponential factor in Eq. (14) is simply a damping factor to suppress the high momentum behavior introduced by p'^L .

It should be noted that our phenomenological contact term M_c can only account for effects that give rise to a smooth energy dependence. Effects such as due to dynamically generated resonances and/or channel couplings [60–63] that give rise to a strong variation of the amplitude as a function of energy cannot be taken into account by the contact term.

Before closing this section, we comment on a feature encountered in describing the reaction (1) within a standard effective Lagrangian approach, like that in Refs. [50, 51], where only the (tree-level) s -, u - and t -channel diagrams are included without the phenomenological contact term. The existing data show backward peaking differential cross sections (see Sec. III), which may indicate a considerable contribution from the u -channel amplitude M_u . In fact, there are a number of Λ and Σ resonances as can be seen in Table I that contribute, in principle, to this reaction. However, it happens that the u -channel resonance contributions, especially, from many of those sub-threshold resonances, also give rise to a total cross section which keeps increasing with energy, a feature that is not supported by the data which reaches a peak and then falls off as a function of energy. Indeed, our model calculation, when those hyperon resonances are considered but without the contact term, exhibits exactly this feature owing to the increasing contribution of the u -channel diagrams with energy. This means that the rescattering term ($V^{\text{NP}} G T^{\text{NP}}$) in the non-pole T -matrix T^{NP} should somehow cancel the increasing contribution from the u -channel resonance amplitudes. Or, perhaps, one needs to consider the u -channel Regge trajectories instead of individual resonances. In the present work, we do not attempt the difficult task of extracting the contributions of these many sub-threshold resonances but, instead, we account for their combined effects with the phenomenological contact term. In any case, it seems that the problem has two scales, one corresponding to the long-range and the other to the short-range dynamics. The latter is, of course, sensitive to the form factors used at the meson-baryon coupling vertices to account for the composite nature of the hadrons and we somehow account for it through the phenomenological contact terms. Problems with two scales have been addressed in the past, where some authors have introduced two form factors, one soft and other hard, to account for such effects [64]. Also, in effective field theories the unknown short-range dynamics is accounted for by contact terms.

We note that the recent calculations by other authors reported in Refs. [50, 51] within usual effective Lagrangian approaches, have dealt with this problem by suppressing the high-energy u -channel contributions. In Ref. [50], this is done by introducing an ad-hoc energy-

³ There are in total four spin matrix elements to describe the reaction (1). However, only two of them, corresponding to the spin-non-flip and spin-flip processes, are independent due to the reflection symmetry about the reaction plane for parity conserving processes. See Ref. [55] for more detailed discussions.

⁴ Here, the phase convention for the associated Legendre function is such that $P_1^1(x) = +\sin(x)$.

⁵ For example, the momentum transfer of this reaction at threshold is about 200 MeV.

TABLE I. The Λ and Σ hyperons listed by the Particle Data Group [17] (PDG) as three- or four-star states. The decay widths and branching ratios of higher-mass resonances ($m_r > 1.6$ GeV) are in a broad range, and the coupling constants are determined from their centroid values. In the present work, the masses (m_r) and widths (Γ_r) of the hyperons as given in this table have been used, except for the $\Sigma(2250)$ resonance. For the latter resonance, see the text.

Λ states					Σ states				
State	m_r (MeV)	Γ_r (MeV)	Rating	$ g_{N\Lambda K} $	State	m_r (MeV)	Γ_r (MeV)	Rating	$ g_{N\Sigma K} $
$\Lambda(1116)$ $1/2^+$	1115.7		****		$\Sigma(1193)$ $1/2^+$	1193		****	
$\Lambda(1405)$ $1/2^-$	1406	50	****		$\Sigma(1385)$ $3/2^+$	1385	37	****	
$\Lambda(1520)$ $3/2^-$	1520	16	****						
$\Lambda(1600)$ $1/2^+$	1600	150	***	4.2	$\Sigma(1660)$ $1/2^+$	1660	100	***	2.5
$\Lambda(1670)$ $1/2^-$	1670	35	****	0.3	$\Sigma(1670)$ $3/2^-$	1670	60	****	2.8
$\Lambda(1690)$ $3/2^-$	1690	60	****	4.0	$\Sigma(1750)$ $1/2^-$	1750	90	***	0.5
$\Lambda(1800)$ $1/2^-$	1800	300	***	1.0	$\Sigma(1775)$ $5/2^-$	1775	120	****	
$\Lambda(1810)$ $1/2^+$	1810	150	***	2.8	$\Sigma(1915)$ $5/2^+$	1915	120	****	
$\Lambda(1820)$ $5/2^+$	1820	80	****		$\Sigma(1940)$ $3/2^-$	1940	220	***	< 2.8
$\Lambda(1830)$ $5/2^-$	1830	95	****		$\Sigma(2030)$ $7/2^+$	2030	180	****	
$\Lambda(1890)$ $3/2^+$	1890	100	****	0.8	$\Sigma(2250)$ $?^?$	2250	100	***	
$\Lambda(2100)$ $7/2^-$	2100	200	****						
$\Lambda(2110)$ $5/2^+$	2110	200	***						
$\Lambda(2350)$ $9/2^+$	2350	150	***						

dependent damping factor in the u -channel resonance diagrams. In Ref. [51] (see, also Ref. [65]) the form factor used in the u -channel diagrams is not an off-shell form factor in that it is not a function of the “off-shellness” ($p_r^2 - m_r^2$) of the propagating hyperon. Moreover, by using a different form of the form factor in the u -channel as compared to that in the s -channel amplitudes, it violates the crossing symmetry already at the tree-level.

III. RESULTS

In this section, we present our results for the reaction $\bar{K} + N \rightarrow K + \Xi$ in different isospin channels. More specifically, we investigate the reactions $K^- + p \rightarrow K^+ + \Xi^-$, $K^- + p \rightarrow K^0 + \Xi^0$, and $K^- + n \rightarrow K^0 + \Xi^-$ considering all the available data on the total and differential cross sections as well as recoil polarization asymmetries.

Before we present our results, we briefly remark on the experimental data considered in this work on total cross sections, differential cross sections, and recoil polarization asymmetries. These data come from different sources of Refs. [30–34, 36, 37, 40] and are available in various forms. Some of them are not in the tabular (numerical) form that can be readily used but are given only in graphical form or as parametrization in terms of the Legendre polynomial expansions. In Ref. [50], Sharov *et al.* have carefully considered the data extraction from these papers. We have checked that the extracted data are consistent with those in the original papers within the permitted accuracy of the check. In the present work, we use these data and no cross sections resulting from the expansion coefficients are considered here.

As mentioned before, there are a number of 3- and 4-star Λ and Σ resonances, including those low-mass sub-threshold ones that contribute, in principle, to the reaction (1). A list for these hyperon resonances and some of their properties is shown in Table I. However, apart from the ground state $\Lambda(1116)$ and $\Sigma(1193)$, for most of these resonances, the required information on the resonance parameters such as the coupling strength (including their signs) to Ξ and/or N are largely unknown. Therefore, the strategy adopted in this work is to consider these parameters as fit parameters and consider the minimum number of resonances required to reproduce the existing data. In particular, we have considered only those resonances that give rise to a considerable contribution to the cross section within a physically reasonable range of the resonance parameter values. More specifically, during the fitting procedure, resonances were added one by one to the model and the quality of fit was checked. It should be mentioned that we have also checked the influence of various combinations of resonances at a time (and not just one by one) to the fit quality. The resonances kept in the presented calculation were those that increased the quality of the fit by a noticeable amount with the variation in χ^2 per data points N , namely, $\delta\chi^2/N > 0.1$. An example of this procedure is shown in Table II where the results of adding one more resonance to the current model, as specified later, is shown. We see that some of these resonances improve somewhat the fit quality of the total cross section but not much the other observables or even worsen the fit quality slightly. We have not included these resonances into our model because the total cross sections suffer from a relatively large uncertainties.

Whenever appropriate, for each resonance considered

TABLE II. Variation in χ^2 per data point N , $\delta\chi^2/N$, obtained when adding one more resonance to the current model (specified in Table. III). A negative $\delta\chi^2/N$ corresponds to an improvement in the result. The quantity $\delta\chi_i^2/N_i$ corresponds to $\delta\chi^2/N$ evaluated for a given type of observable specified by index i : $i = \sigma$ (total cross section), $= d\sigma$ (differential cross section) and, $= P$ (recoil asymmetry). $N = N_\sigma + N_{d\sigma} + N_P$ denotes the total number of data points. Furthermore, $\delta\chi_i^2/N_i$ is given for the charged Ξ^- ($\delta\chi_-^2/N_-$) and neutral Ξ^0 ($\delta\chi_0^2/N_0$) production processes, separately. The last column corresponds to $\delta\chi^2/N$ of the global fit considering all the data of both reaction processes. The last row corresponds to χ_i^2/N_i of the current model.

	$\bar{K}^- + p \rightarrow K^+ + \Xi^-$				$\bar{K}^- + p \rightarrow K^0 + \Xi^0$				
Y added	$\delta\chi_\sigma^2/N_\sigma$	$\delta\chi_{d\sigma}^2/N_{d\sigma}$	$\delta\chi_P^2/N_P$	$\delta\chi_-^2/N_-$	$\delta\chi_\sigma^2/N_\sigma$	$\delta\chi_{d\sigma}^2/N_{d\sigma}$	$\delta\chi_P^2/N_P$	$\delta\chi_0^2/N_0$	$\delta\chi^2/N$
$\Lambda(1405)$	-0.01	0.03	0.00	-0.01	0.03	0.00	0.02	0.01	0.00
$\Lambda(1600)$	-0.02	0.00	-0.01	-0.01	0.02	0.00	0.02	0.01	0.00
$\Lambda(1670)$	-0.01	0.00	0.00	0.00	0.02	0.00	0.02	0.01	0.00
$\Lambda(1800)$	0.00	0.01	0.00	0.00	-0.01	0.00	0.01	0.00	0.00
$\Lambda(1810)$	-0.01	-0.01	0.00	-0.01	0.02	0.00	0.02	0.01	0.00
$\Lambda(1520)$	-0.06	0.02	0.00	0.00	-0.05	-0.01	0.00	-0.02	0.00
$\Lambda(1690)$	0.00	0.00	0.00	0.00	0.00	0.00	0.00	0.00	0.00
$\Lambda(1820)$	-0.08	0.01	0.01	0.00	-0.07	0.00	-0.02	-0.02	-0.01
$\Lambda(1830)$	-0.05	0.01	0.01	0.00	0.00	0.02	0.02	0.01	0.00
$\Lambda(2110)$	-0.02	0.02	0.01	0.01	-0.03	-0.01	-0.03	-0.02	0.00
$\Lambda(2100)$	-0.08	0.04	0.03	0.02	-0.04	-0.02	-0.01	-0.03	0.01
$\Sigma(1660)$	-0.02	0.00	0.00	0.00	-0.01	0.01	0.00	0.01	0.00
$\Sigma(1750)$	-0.01	0.01	0.00	0.00	-0.01	0.01	0.00	0.00	0.00
$\Sigma(1670)$	-0.01	0.00	-0.01	0.00	0.02	0.01	0.01	0.01	0.00
$\Sigma(1940)$	0.02	0.00	0.01	0.00	0.01	-0.01	0.01	-0.01	0.00
$\Sigma(1775)$	-0.01	0.01	0.04	0.01	-0.02	0.00	-0.02	-0.01	0.00
$\Sigma(1915)$	0.01	-0.01	0.00	-0.01	-0.03	0.00	0.00	-0.01	-0.01
	χ_σ^2/N_σ	$\chi_{d\sigma}^2/N_{d\sigma}$	χ_P^2/N_P	χ_-^2/N_-	χ_σ^2/N_σ	$\chi_{d\sigma}^2/N_{d\sigma}$	χ_P^2/N_P	χ_0^2/N_0	χ^2/N
	1.53	1.64	1.85	1.64	0.88	1.06	1.73	1.10	1.49

in this work, the corresponding coupling constants g_{KYN} and $g_{KY\Xi}$ were constrained in such way that the sum of the branching ratios $\beta_{Y \rightarrow KN} + \beta_{Y \rightarrow K\Xi}$ not to exceed unit. Because, within our model, the data are sensitive only to the product of the coupling constants $g_{KYN}g_{KY\Xi}$, setting $|g_{KYN}| = |g_{KY\Xi}|$ for the purpose of estimating the individual branching ratios, and only for this purpose, is a simple way of keeping our coupling constant values within a physically acceptable range. Admittedly, the currently existing data are limited and suffer from large uncertainties, thus an accurate determination of the resonance parameters are not possible at this stage. For this, one needs to wait for new more precise data, possibly including more spin polarization data. In this regard, the multi-strangeness baryon spectroscopy program using the anti-kaon beam at J-PARC will be of particular relevance. For the ground states $\Lambda(1116)$ and $\Sigma(1193)$, the corresponding coupling constants are estimated based on the flavor SU(3) symmetry relations [23].

The phenomenological contact amplitude M_c contains two sets of free parameters, $\{g_1^{LT}, \alpha_L^T\}$ and $\{g_2^{LT}, \beta_L^T\}$, to be fixed by adjusting to reproduce the experimental data, for a given set of $\{L, T\}$ as shown in Eq. (14). In order to reduce the number of free parameters, we have assumed the parameter α_L^T to be equal to β_L^T and independent on T and L , i.e., $\alpha_L^T = \beta_L^T = \alpha$. The scale pa-

rameter Λ_S has been fixed as $\Lambda_S = 1$ GeV. Note that the phenomenological contact amplitude can and should be complex in principle, since it accounts for the rescattering contribution ($V^{\text{NP}}GT^{\text{NP}}$) of the non-pole T -matrix which is complex in general. Accordingly, the coupling strength parameters g_1^{LT} and g_2^{LT} are complex quantities. In order to reduce the number of free parameters, we take their phases to be independent on L and T , so that, $\{\phi_a\}_L^T = \phi_a$ and $\{\phi_b\}_L^T = \phi_b$ for all the sets $\{L, T\}$. Also, in the present calculation, we find that it suffices to consider partial waves up to $L = 2$ in the contact amplitude to reproduce the existing data.

The resonances included in the present model calculations and the corresponding resonance parameters are displayed in Table III as well as the parameters of the phenomenological contact term M_c . We do not give the associated uncertainties here because they are not well constrained. In the present calculation, resonances with $J \leq 7/2$ were considered. The masses and the total widths of the resonances are taken to be those quoted in PDG [17] and are given in Table I, except for the mass of the $\Sigma(2250)$ resonance. Currently, the $\Sigma(2250)$ resonance is not well established and have a three-star status [17]. In fact, the PDG doesn't even assign the spin-parity quantum numbers for this resonance. The analyses of Ref. [39], actually show as two possible resonances, one

TABLE III. Fitted parameter values of the current model. For the details of the resonance parameters, see the Appendix. For the contact amplitude, see Eq. (14). The entries in boldface are taken from Ref. [23] and they are not fit parameters. Here, it is assumed that $\{\phi_a\}_L^T = \phi_a$ and $\{\phi_b\}_L^T = \phi_b$, in addition to $\alpha_L^T = \beta_L^T = \alpha$.

Y	$g_{N\Lambda K}$	$\lambda_{N\Lambda K}$	$g_{\Xi\Lambda K}$	$\lambda_{\Xi\Lambda K}$	Λ (MeV)								
$\Lambda(1116)\frac{1}{2}^+$	-13.24	1.0	3.52	1.0	900								
$\Sigma(1193)\frac{1}{2}^+$	3.58	1.0	-13.26	1.0	900								
	$g_{N\Lambda K}$	$g_{\Xi\Lambda K}$	$\lambda_{N\Lambda K}$	-	$\lambda_{\Xi\Lambda K}$	Λ (MeV)	L	a_L^0	a_L^1	b_L^0	b_L^1	ϕ_a	ϕ_b
$\Lambda(1890)\frac{3}{2}^-$	-0.11					900	0	0.28	-1.18				
$\Sigma(1385)\frac{3}{2}^+$	18.76	1.0			1.0	900	1	3.22	-4.84	3.40	-0.60		
$\Sigma(2030)\frac{7}{2}^+$	0.49					900	2	3.06	21.08	-9.40	2.28		
$\Sigma(2250)\frac{5}{2}^-$	-0.033					900	$\Lambda_S = 1$ GeV		$\alpha = 3.62$		0.22	-0.16	

with $J^P = 5/2^-$ at about 2270 ± 50 MeV and another with $J^P = 9/2^-$ at about 2210 ± 30 MeV. In the present work we have assumed $\Sigma(2250)$ to have $J^P = 5/2^-$ with the mass of 2265 MeV. This is motivated by the fact that the total cross section in $K^- + p \rightarrow K^+ + \Xi^-$ shows a small bump structure at around 2300 MeV, which is well reproduced in our model with the mass of $\Sigma(2250)$ adjusted to be at 2265 MeV. For the corresponding width, we have adopted the value quoted in PDG as shown in Table I.

All the parameters of the present model calculation are determined as described above and we now present the results obtained in our model. The overall fit quality is quite good with $\chi^2/N = 1.49$ as displayed in Table II. There we also show the partial χ_i^2/N_i evaluated for a given type of observable specified by the index i as explained in the caption of Table II. In Fig. 2 we show the results for the total cross section in the charged Ξ production reaction from the proton target, i.e., $K^- + p \rightarrow K^- + \Xi^-$, for the center-of-mass energies up to $W = 3$ GeV. Figure 2(a) displays the total contribution which reproduces the data rather well. The dynamical content of the present model is also shown in the same figure. We find that the contact term rises quickly from threshold peaking at around 2.1 GeV and falls off more slowly as energy increases. It dominates largely the cross section except for energies very close to threshold and above ~ 2.7 GeV, where the hyperon resonance contributions are comparable. The Λ hyperons contribution is strongest near threshold and dies off very slowly as energy increases. The Σ contribution is relatively small over the entire energy range considered, except in the interval of 2.0–2.3 GeV, where it becomes comparable to the Λ contribution. Near threshold, there is a strong destructive interference between the contact term and (mainly) the Λ hyperons contribution. At higher energies, the data indicates an existence of a bump structure at $W \sim 2.3$ GeV. Our model reproduces this feature due to a delicate destructive and constructive interference of the contact term and the hyperon resonance contributions as the energy increases. We also mention that we have explored the possibility of a much smaller contact amplitude contribution than shown in Fig. 2(a) consid-

ering various different sets of hyperon resonances from Table I; however, we were unable to find a solution with a comparable fit quality to that of Fig. 2(a).

Figure 2(b) displays the individual Λ hyperon contributions. We see that the ground state $\Lambda(1116)$ is, by far, the dominant contribution which is due to the tail of the corresponding u -channel process. Analogously, the individual Σ hyperon contributions are shown in Fig. 2(c). Here, the relatively small cross section near threshold is due to the destructive interference between the $\Sigma(1192)$ and $\Sigma(1385)$. The enhancement of the cross section in the energy interval of 2.0–2.3 GeV is basically due to the $\Sigma(2030)$ resonance. The $\Sigma(2250)$ leads to a little shoulder in the total Σ contribution. We note that any non-negligible contribution from the hyperons for energies above ~ 2.3 GeV is due to the u -channel processes.

In Fig. 3 we show the total cross section results for the neutral Ξ production process, $K^- + p \rightarrow K^0 + \Xi^0$. Here, the data are of such poor quality that they impose much less constraint on the model parameters than the corresponding data in the charged Ξ^- production. Here, the resulting dynamical content shown in Fig. 3(a) is similar to that for the charged Ξ^- production discussed above, i.e., it is largely dominated by the contact term. However, we see a quite different feature in the Λ and Σ resonance contributions as compared to that for the charged Ξ^- production [cf. Fig. 2(a)]. One notable difference between the charged and neutral Ξ production reactions considered here is that the u -channel Λ hyperon contribution is absent in the Ξ^0 production case. Also, the relative contribution of the Σ hyperons is much larger in the neutral Ξ^0 production than in the charged Ξ^- production, especially, in the near threshold region.

Figures 3(b) and 3(c) show the individual hyperon contributions. As mentioned before, due to the absence of the u -channel Λ exchange in the neutral Ξ^0 production, the $\Lambda(1116)$ contribution is insignificant, leading to a negligible contribution of the Λ hyperons. Due to the isospin factors, here, the $\Sigma(1192)$ and $\Sigma(1385)$ hyperons interfere constructively, especially, near the threshold. Recall that, for charged Ξ^- production, these hyperons interfere destructively [cf. Fig. 2(c)].

In Fig. 4 we illustrate the amount of the above-

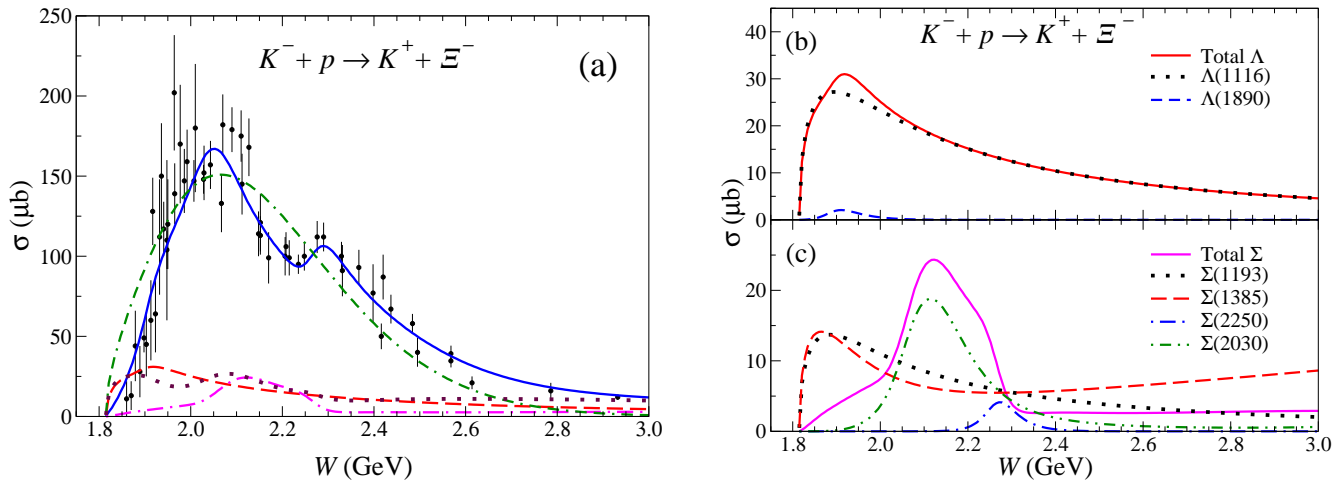


FIG. 2. (Color online) Total cross section for the $K^- + p \rightarrow K^+ + \Xi^-$ reaction. (a) The solid blue line represents the result of the full calculation of the present model. The red dashed line shows the combined Λ hyperons contribution. The magenta dash-dotted line shows the combined Σ hyperons contribution. The brown dotted line shows the combined Λ and Σ hyperons contribution. The green dash-dash-dotted line corresponds to the contact term. (b) The solid red line represents the combined Λ hyperons contribution that is the same as the red dashed line in (a). The dotted and dashed lines show the $\Lambda(1116)$ and $\Lambda(1890)$ contributions, respectively. (c) The solid magenta line represents the combined Σ hyperons contribution that is the same as the magenta dash-dotted line in (a). The dotted, dashed, and dot-dot-dashed lines show the contributions from the $\Sigma(1193)$, $\Sigma(1385)$, $\Sigma(2250)$, and $\Sigma(2030)$, respectively. The experimental data (black circles) are the digitized version as quoted in Ref. [50] from the original work of Refs. [29–34, 36–39, 41–43].

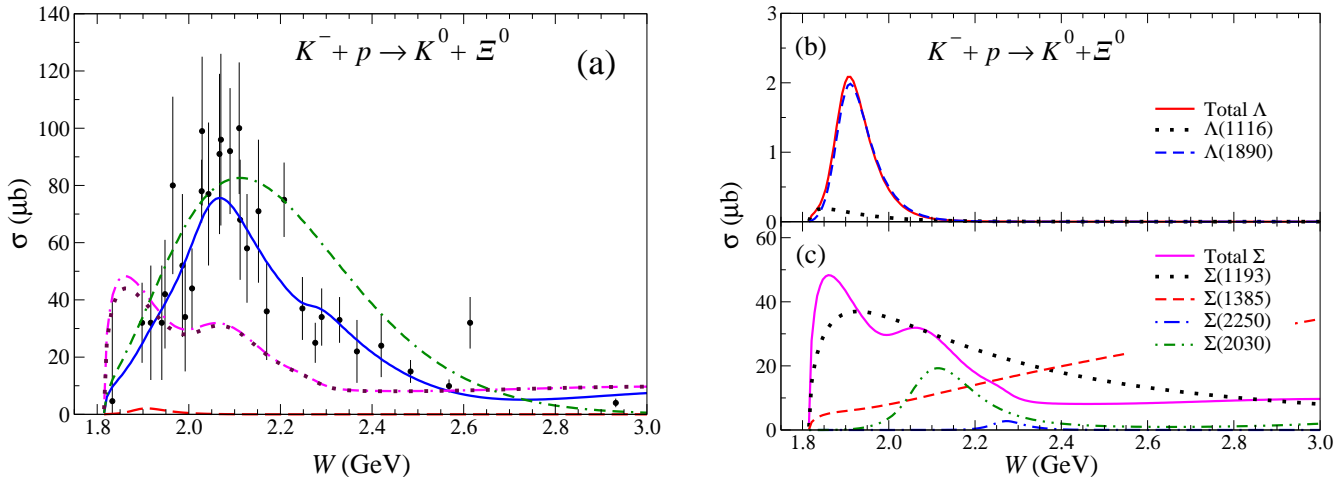


FIG. 3. (Color online) Same as Fig. 2 for the $K^- + p \rightarrow K^0 + \Xi^0$ reaction. The experimental data (black circles) are the digitized version as quoted in Ref. [50] from the original work of Refs. [30, 37–40, 43].

threshold resonance contributions of the present model to the total cross sections by switching them off one by one with respect to the full results shown in Figs. 2(a) and 3(a). We see in Fig. 4(a) that the $\Sigma(2030)$ affects most the cross sections in the range of $W \sim 2.0$ to 2.4 GeV. This resonance is clearly needed in our model to reproduce the data. It also affects the recoil polarization as will be discussed later. It should be mentioned that this resonance also helps to reproduce the measured $K^+\Xi^-$ invariant mass distribution in $\gamma p \rightarrow K^+K^+\Xi^-$ [24], by filling in the valley in the otherwise double-bump structured invariant mass distribution, a feature that is not

observed in the data [66]. The $\Lambda(1890)$ affects the total cross section in the range of $W \sim 1.9$ to 2.1 GeV and the $\Sigma(2250)5/2^-$ around $W \sim 2.2$ GeV to reproduce the observed bump structure. A more accurate data set is clearly needed for a more definitive answer about the role of the $\Lambda(1890)$ and $\Sigma(2250)$ resonances. Figure 4(b) for the neutral Ξ^0 production shows also a similar feature observed in the Ξ^- case for the $\Sigma(2030)$ resonance. Here, the influence of the $\Sigma(2250)5/2^-$ is smaller and that of the $\Lambda(1890)$ is hardly seen. Recall that there is no u -channel Λ contribution in the neutral Ξ^0 production.

The results for differential cross sections in both $K^- +$

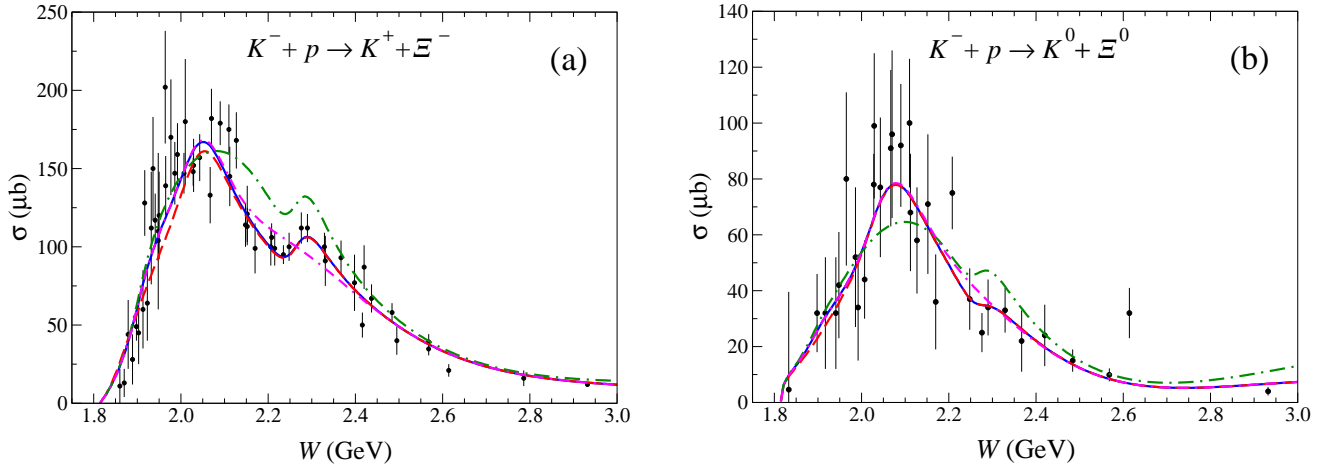


FIG. 4. (Color online) Total cross section results with individual resonances switched off (a) for $K^- + p \rightarrow K^+ + \Xi^-$ and (b) for $K^- + p \rightarrow K^0 + \Xi^0$. The blue lines represent the full result shown in Figs. 2 and 3. The red dashed lines, which almost coincide with the blue lines represent the result with $\Lambda(1890)$ switched off. The green dash-dotted lines represent the result with $\Sigma(2030)$ switched off and the magenta dash-dash-dotted lines represent the result with $\Sigma(2250)5/2^-$ switched off.

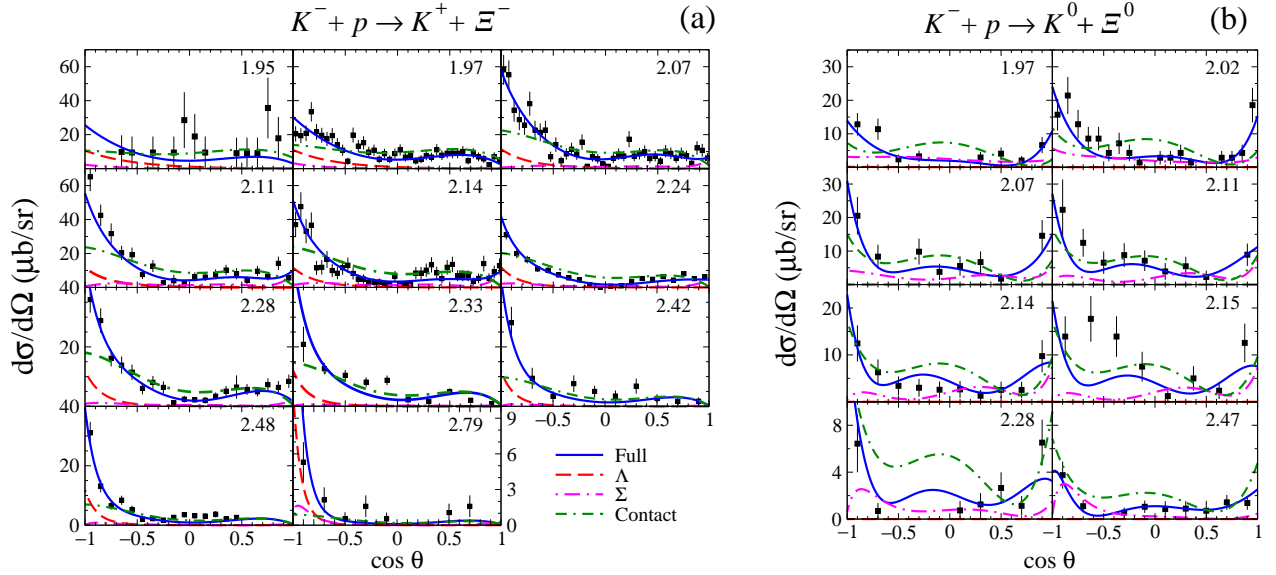


FIG. 5. (Color online) Kaon angular distributions in the center-of-mass frame (a) for $K^- + p \rightarrow K^+ + \Xi^-$ and (b) for $K^- + p \rightarrow K^0 + \Xi^0$. The blue lines represent the full model results. The red dashed lines show the combined Λ hyperons contribution. The magenta dash-dotted lines show the combined Σ hyperons contribution. The green dash-dash-dotted line corresponds to the contact term. The numbers in the upper right corners correspond to the centroid total energy of the system W . Note the different scales used. The experimental data (black circles) are the digitized version as quoted in Ref. [50] from the original work of Refs. [31–34, 36, 37] for the $K^- + p \rightarrow K^+ + \Xi^-$ reaction and of Ref. [30, 36, 37, 40] for the $K^- + p \rightarrow K^0 + \Xi^0$ reaction.

$p \rightarrow K^+ + \Xi^-$ and $K^- + p \rightarrow K^0 + \Xi^0$ are shown in Figs. 5(a) and 5(b), respectively, in the energy domain up to $W = 2.8$ GeV for the former and up to $W = 2.5$ GeV for the latter reaction. Overall, the model reproduces the data quite well. There seem to be some discrepancies for energies $W = 2.33$ to 2.48 GeV in the charged Ξ^- production. Our model underpredicts the yield around $\cos \theta = 0$. As in the total cross sections, the data for the neutral Ξ^0 production are fewer and less accurate than

for the charged Ξ^- production. In particular, the Ξ^0 production data at $W = 2.15$ GeV seems incompatible with those at nearby lower energies and that the present model is unable to reproduce the observed shape at backward angles. It is clear from Figs. 5(a) and 5(b) that the charged channel shows a backward peaked angular distributions, while the neutral channel shows enhancement for both backward and forward scattering angles (more symmetric around $\cos \theta = 0$) for all but perhaps the high-

est energies. In the charged Ξ^- production, both the resonance and contact amplitude contributions are backward angle peaked and, as the energy increases, they get smaller and smaller at forward angles. In Ξ^0 production, both the Σ resonance and contact amplitude contributions also exhibit an enhancement for forward angles. Note that the Λ resonance contribution here is negligible due to the absence of the u -channel process. The interference pattern in the forward angular region depends on energy. At lower energies the interfere is constructive and it becomes destructive at higher energies. The behavior of the angular distributions in terms of the partial waves will be discussed later in connection to the results of Figs. 6(b) and 8(b).

The partial-wave content in the cross sections for the charged Ξ^- production process arising from the present model is shown in Figs. 6(a) and 6(b). As can be seen in Fig. 6(a), the total cross section is dominated by the P and D waves in almost the entire range of energy considered, even at energies very close to threshold where one sees a strongly raising P -wave contribution. The S -wave contribution is very small. This peculiar feature is caused by the ground state $\Lambda(1116)$, whose contribution cancels to a large extent the otherwise dominant S -wave contribution close to threshold, in addition to enhancing the P -wave contribution. One way of probing the S -wave content close to threshold in a model-independent manner is to look at the quantity σ/p' as a function of p'^2 , where p' is the relative momentum of the final $K\Xi$ state. The reason to look at this quantity is that, for hard processes, the partial wave reaction amplitude goes basically with p'^L for a given orbital angular momentum L as mentioned in Sec. II. This leads to

$$\frac{\sigma}{p'} = c_0 + c_1 p'^2 + c_2 p'^4 + \dots, \quad (15)$$

where c_L 's are constants. Figure 7 illustrates this point. Although the existing experimental data are of poor quality, they reveal the general features just mentioned. In particular, for the charged Ξ^- production process, the data indicate a linear dependence of σ/p' close to threshold implying a strong P -wave contribution. The present model result is consistent with this behavior. The corresponding results for the neutral Ξ^0 production are also shown in Fig. 7. There, the data are scattered around but are consistent with the S -wave dominance and our model just shows this feature [see also Fig. 8(a)]. In Fig. 6(a) we also see a small F -wave contribution above $W \sim 2.0$ GeV and practically saturates the total cross section for energies considered. Note that since our contact term includes the partial waves through the D waves only, the F -wave contribution is entirely due to the hyperon resonances. The enhancement of the D -wave contribution around $W = 2.3$ GeV as well as the little shoulder in the P -wave contribution are due to the $\Sigma(2250)$ hyperon. Of course, the partial wave contributions are constrained dominantly by the differential cross section and they are shown in Fig. 6(b). As mentioned before, the shape of the angular distribution is backward-angle peaked and that

the cross section is very small at forward angles. This behavior is a direct consequence of the very significant interference between the P and D waves. This can be seen by expanding the cross section in partial waves. Considering the partial waves through $L = 2$ and following Ref. [55], the differential cross section may be expressed as

$$\begin{aligned} \frac{d\sigma}{d\Omega} = & \left[|\alpha_{02}|^2 + (|\alpha_1|^2 + \alpha_{02}\alpha_2^*) \cos^2 \theta + |\alpha_2|^2 \cos^4 \theta \right. \\ & \left. + (|\beta_1|^2 + |\tilde{\beta}_2|^2 \cos^2 \theta) \sin^2 \theta \right] \\ & + 2 \operatorname{Re} \left[\alpha_{02}\alpha_1^* + \alpha_1\alpha_2^* \cos^2 \theta + \beta_1\tilde{\beta}_2^* \sin^2 \theta \right] \cos \theta, \end{aligned} \quad (16)$$

where the coefficients α_L (β_L) denotes a linear combination of the partial-wave matrix elements corresponding to the spin-non-flip (spin flip) process with a given orbital angular momentum L [see Eq. (13)]. Here, $\alpha_{02} \equiv \alpha_0 - \frac{1}{3}\alpha_2$ and $\tilde{\beta}_2 \equiv 2\beta_2$. In the above equation, the last term on the right hand side which involves an interference between the P and D waves is an odd function in $\cos \theta$, while the other term (in big brackets) is an even function. These two terms cancel each other to a large extent at forward angles while at backward angles they add up. Note that these partial waves are comparable in strength as shown in Fig. 6(a) so that their interference term leading to an odd function part can largely cancel the even term at forward angles.

Figures 8(a) and 8(b) display the partial wave content in the cross sections for the neutral Ξ^0 production process. In contrast to the charged Ξ^- production, here one sees that the largest contribution to the total cross section is the D -wave and that the P -wave is largely suppressed, which is a direct consequence of the shape of the observed angular distribution whose partial wave contributions are shown in Fig. 8(b). There, compared to that for charged Ξ^- , one sees a more symmetric angular shape about $\cos \theta = 0$ that is dominated by the D -wave. The present model reproduces the observed behavior of the K^0 angular distribution by suppressing the P -wave contribution as can be easily understood from Eq. (16). The rather drastic suppression of the P wave can be better seen in Fig. 8(a). For energies very close to threshold, the cross section is dominated by the S -wave as seen also in Fig. 8(a).

The results for the recoil polarization asymmetry multiplied by the cross section are shown in Fig. 9 in the energy interval of $W = 2.1$ to 2.5 GeV. Overall, we reproduce the data reasonably well. We also find that the results shown at $W = 2.11$ GeV are still significantly affected by $\Sigma(2030)$. This corroborates the findings of Ref. [50]. We recall that the recoil asymmetry is proportional to the imaginary part of the product of the non-spin-flip matrix element (M_{ss}) with the complex conjugate of the spin-flip matrix element ($M_{s's}$ with $s' \neq s$) [55], so that it vanishes identically unless these matrix elements are complex with non-vanishing real and imag-

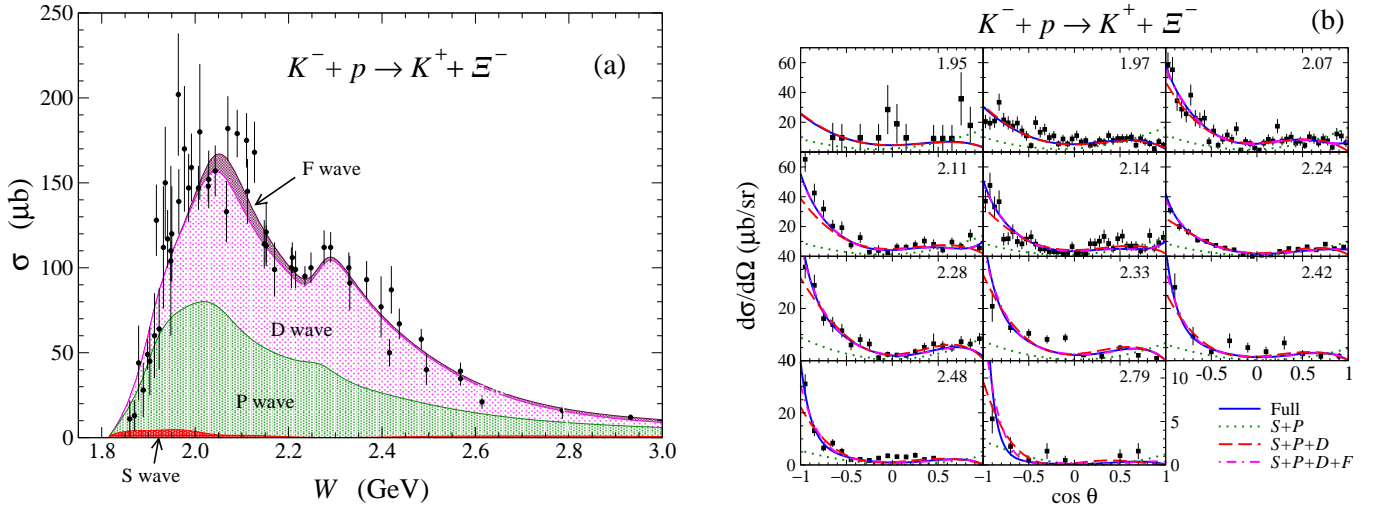


FIG. 6. (Color online) Partial wave decomposition of the total cross section and the angular distribution for $K^- + p \rightarrow K^+ + \Xi^-$. (a) Total cross section sectioned by contributions from each partial wave L . The red shaded area indicates the S -wave contribution, while the green area corresponds to the P -wave. Magenta indicates the D -wave and maroon the F -wave. (b) K^+ angular distribution: the solid blue lines are the full results, while the dotted green lines represent the sum of $S + P$ waves, the red dashed lines represent the $S + P + D$ waves and the dash-dotted magenta lines represent the $S + P + D + F$ waves. For lower energies, the $S + P + D$ waves already saturate the full cross section results so that the F - and higher-wave contributions cannot be distinguished from the full result.

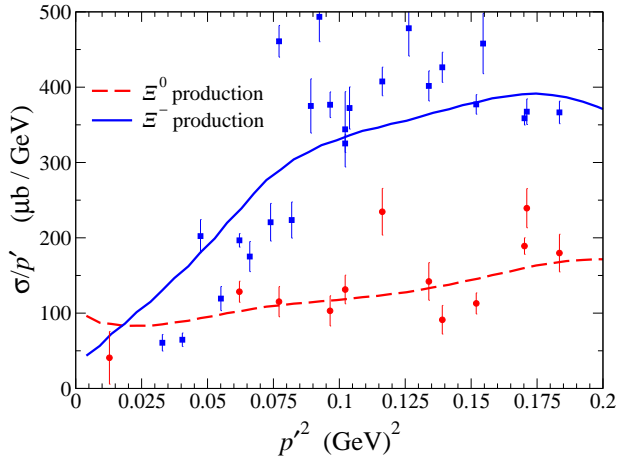


FIG. 7. (Color online) Ratio of the measured total cross section σ and the final state $K\Xi$ relative momentum p' as a function of p'^2 . The blue square data correspond to $K^- + p \rightarrow K^+ + \Xi^-$, while the red circle data to $K^- + p \rightarrow K^0 + \Xi^0$. The blue solid and red dashed curves are the present model results corresponding to $K^- + p \rightarrow K^+ + \Xi^-$ and $K^- + p \rightarrow K^0 + \Xi^0$, respectively.

inary parts. We can therefore expect the recoil polarization to be sensitive to the complex nature of the reaction amplitude, in particular, to the phenomenological contact amplitude M_c introduced in the present model. Indeed, if one forces the coupling strength parameters g_1^{LT} and g_2^{LT} in Eq. (14) to be pure real during the fitting procedure, the χ^2_P/N_P deteriorates, e.g., from 1.85 to 2.25 for the $K^- + p \rightarrow K^+ + \Xi^-$ reaction, although

the quality of fit for cross sections is nearly unchanged.

In Fig. 10 we show the present model predictions for the target-beam asymmetries K_{xx} and K_{xz} multiplied by the unpolarized cross section, i.e., $\frac{d\sigma}{d\Omega} K_{xx}$ and $\frac{d\sigma}{d\Omega} K_{xz}$ for both the charged Ξ^- and neutral Ξ^0 production processes. Note that these target-recoil asymmetries, together with K_{yy} , are the only three independent double-spin observables in the reaction of Eq. (1) as discussed in Ref. [55]. Indeed, the only two other non-vanishing target-recoil asymmetries are related by $K_{zz} = K_{xx}$ and $K_{zx} = -K_{xz}$.⁶ We mention that $\frac{d\sigma}{d\Omega} K_{xx}$ is proportional to the difference of the magnitude squared of the spin-non-flip and spin-flip matrix elements, while $\frac{d\sigma}{d\Omega} K_{xz}$ is proportional to the real part of the product of the spin-non-flip matrix element with the complex conjugate of the spin-flip matrix element. Therefore, unlike the recoil asymmetry, these spin observables do not vanish even if the reaction amplitude is pure real or pure imaginary. This means that they are, like the cross section, much less sensitive to the complex nature of the phenomenological contact amplitude.

To gain some insight into the angular dependence exhibited by these target-recoil asymmetries in Fig. 10, we

⁶ Note that the symmetry of the reaction leads to $K_{yy} = \pi_{\Xi}$ independent on the scattering angle θ [54, 55]. Here, π_{Ξ} stands for the parity of the produced Ξ which is taken to be $\pi_{\Xi} = +1$ for the ground state Ξ . Also, $K_{xx} = K_{zz}|_{\cos\theta=\pm 1} = \pi_{\Xi}$. The target asymmetry is identical to the recoil asymmetry in the present reaction. Therefore, we exhaust all the independent observables available in the reaction processes considered here.

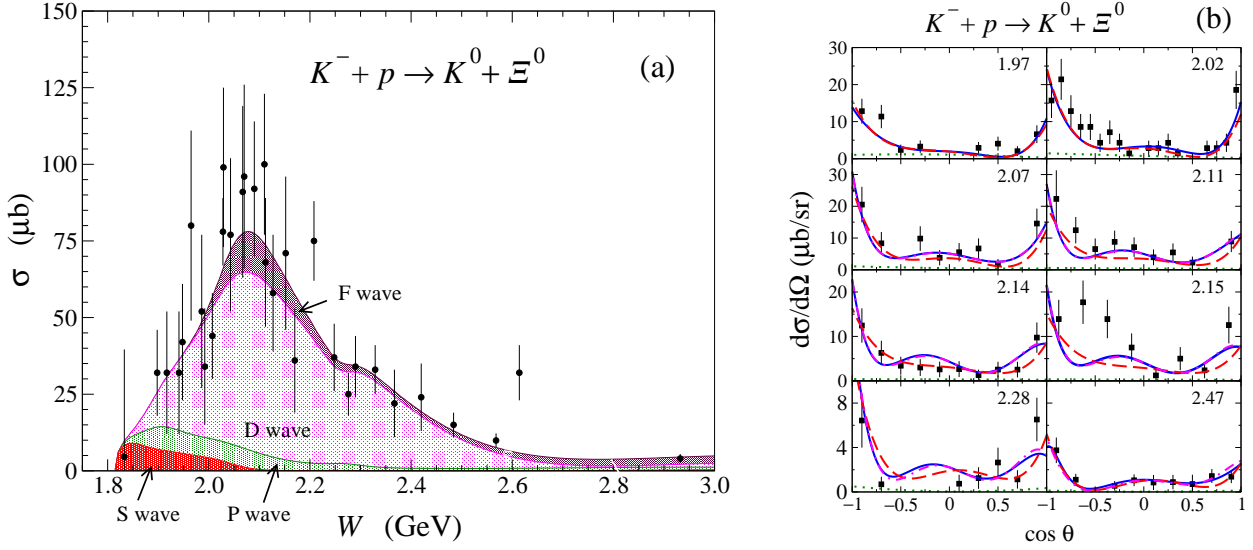


FIG. 8. (Color online) Same as in Fig. 6 but for $K^- + p \rightarrow K^0 + \Xi^0$.

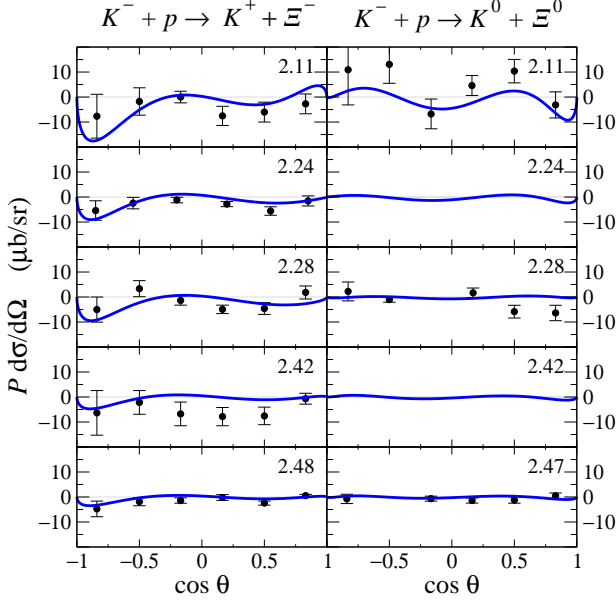


FIG. 9. (Color online) The recoil asymmetry $\frac{d\sigma}{d\Omega}P$ for both the $K^- + p \rightarrow K^+ + \Xi^-$ and $K^- + p \rightarrow K^0 + \Xi^0$ reactions. The blue solid lines represent the full results of the current model. Data are from Refs. [33, 37].

express them in terms of partial waves with $L \leq 2$. We have

$$\begin{aligned} \frac{d\sigma}{d\Omega} K_{xx} = & \left[|\alpha_{02}|^2 + (|\alpha_1|^2 + \alpha_{02}\alpha_2^*) \cos^2 \theta + |\alpha_2|^2 \cos^4 \theta \right. \\ & \left. - (|\beta_1|^2 + |\tilde{\beta}_2|^2 \cos^2 \theta) \sin^2 \theta \right] \\ & + 2 \operatorname{Re} \left[\alpha_{02}\alpha_1^* + \alpha_1\alpha_2^* \cos^2 \theta - \beta_1\tilde{\beta}_2^* \sin^2 \theta \right] \cos \theta, \end{aligned} \quad (17a)$$

$$\begin{aligned} \frac{d\sigma}{d\Omega} K_{xz} = & 2 \operatorname{Re} \left[\alpha_{02}\beta_1^* + (\alpha_1\tilde{\beta}_2^* + \alpha_2\beta_1^*) \cos^2 \theta \right. \\ & \left. + (\alpha_{02}\tilde{\beta}_2^* + \alpha_1\beta_1^*) \cos \theta + \alpha_2\tilde{\beta}_2^* \cos^3 \theta \right] \sin \theta. \end{aligned} \quad (17b)$$

Note that the only difference between $\frac{d\sigma}{d\Omega} K_{xx}$ given above and differential cross section given by Eq. (16) is the sign change of the terms involving β_L . These terms are, however, proportional to $\sin^2 \theta$. Therefore, this spin observable behaves like the differential cross section at very forward and backward angles, where $\sin^2 \theta \ll 1$. At $\cos \theta = 0$, the difference is due to the term of $\pm |\beta_1|^2$ which is a P -wave contribution in the spin-flip amplitude. Now, if we ignore the P -wave contribution — which is relatively very small in the neutral Ξ^0 production over the nearly entire energy region considered as seen in Fig. 8(a) — it is immediate to see that Eq. (17a) involves only terms that are symmetric about $\cos \theta = 0$. We see in Fig. 10(b) that $\frac{d\sigma}{d\Omega} K_{xx}$ exhibits roughly this symmetry.

For $\frac{d\sigma}{d\Omega} K_{xz}$, Eq. (17b) reveals a rather complicated angular dependence in general, and no particular feature is apparent in the results shown in Fig. 10, especially for the charged Ξ^- production process. Neglecting the P -wave contribution, Eq. (17b) reduces to $\frac{d\sigma}{d\Omega} K_{xz} = \operatorname{Re} \left[(\alpha_{02} + \alpha_2 \cos^2 \theta) \tilde{\beta}_2^* \right] \sin 2\theta$, which is roughly the angular dependence exhibited in Fig. 10(b).

The present model predictions for the $K^- + n \rightarrow K^0 + \Xi^-$ reaction are shown in Fig. 11. Here, the experimental data are extremely scarce and they were not included in the present fitting procedure. Nevertheless, the current model is seen to predict those few data quite reasonably. Both the total and differential cross sections exhibit a very similar feature to those of the $K^- + p \rightarrow K^+ + \Xi^-$ reaction with a noticeable small enhancement in the differential cross sections as seen in Fig. 11(b) for forward

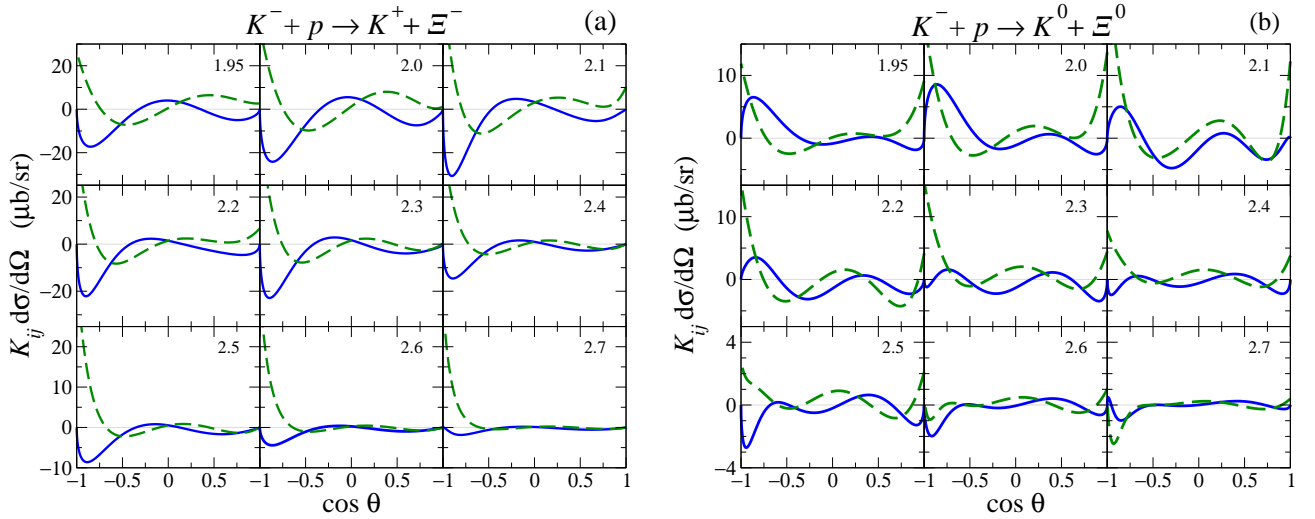


FIG. 10. (Color online) Target-recoil asymmetries K_{xx} (green dashed curves) and K_{xz} (blue solid curves) as defined in Ref. [55] for the reactions (a) $K^- + p \rightarrow K^+ + \Xi^-$ and (b) $K^- + p \rightarrow K^0 + \Xi^0$. The numbers in the upper right corners represent the total energy of the system W in units of GeV.

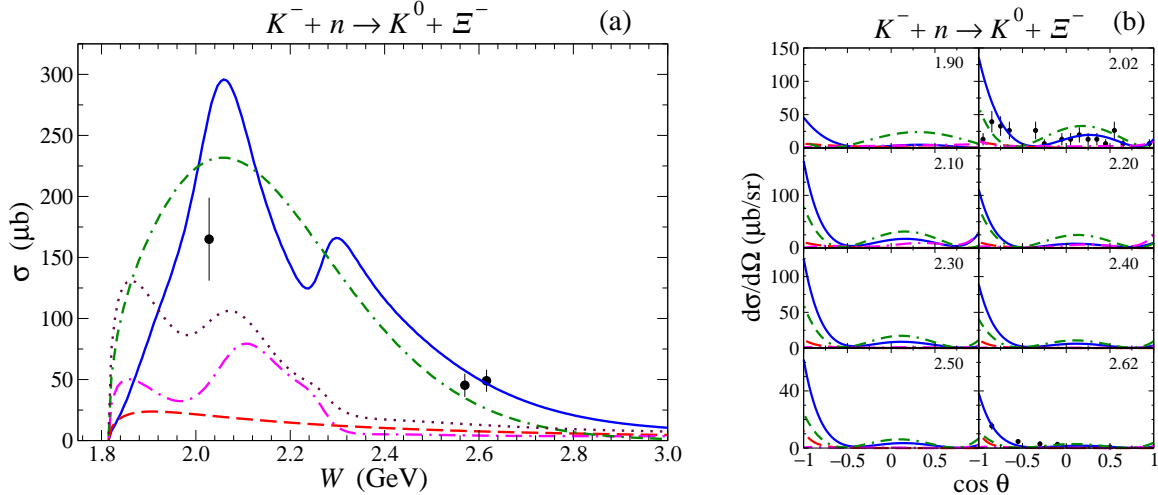


FIG. 11. (Color online) Same as Figs. 2(a) and 5 for the $K^- + n \rightarrow K^0 + \Xi^-$ reaction. The experimental data are from Refs. [30, 38].

angles near $\cos \theta = 0$ in $K^- + n \rightarrow K^0 + \Xi^-$. We see, however, some bigger differences in the individual amplitude contributions, more clearly seen in the total cross sections that are given in Fig. 11(a). There, the Σ hyperon contribution is larger than the Λ contribution over the entire energy region up to $W \sim 2.3$ GeV, in particular, at low energies near threshold. This is due to the absence of the strong destructive interference between the $\Sigma(1385)$ and $\Sigma(1192)$ (not shown), since the latter hyperon contribution is suppressed to a large extent compared to the case of $K^- + p \rightarrow K^+ + \Xi^-$. Moreover, there is a constructive interference with the Λ hyperon, which makes the sum of the hyperons contribution relatively large in the low energy region.

IV. CONCLUSION

In this work we have presented our analysis on the reaction of $K^- + N \rightarrow K + \Xi$ within an effective Lagrangian approach that includes a phenomenological contact term to account for the rescattering contribution of the non-pole part of the reaction amplitude in the Bethe-Salpeter equation and for other possible (short-range) dynamics that are not taken into account explicitly in the model. By introducing the phenomenological contact term, we avoid the problem of a strong u -channel hyperon contribution which keeps growing as a function of energy leading to ever increasing cross sections, a common feature of the effective Lagrangian approaches. The present model also includes the $\Lambda(1890)$, $\Sigma(1385)$, $\Sigma(2030)$, and

$\Sigma(2250)$ resonance contributions apart from the ground states $\Lambda(1116)$ and $\Sigma(1193)$.

The available total and differential cross sections, as well as the recoil asymmetry data, in both the $K^- + p \rightarrow K^+ + \Xi^-$ and $K^- + p \rightarrow K^0 + \Xi^0$ processes are well reproduced by the present model. We have found that the above-threshold resonances $\Lambda(1890)$, $\Sigma(2030)$, and $\Sigma(2250)$ are required to achieve a good fit quality of the data. Among them, the $\Sigma(2030)$ resonance is the most critical one. This resonance affects not only the cross sections but also the recoil asymmetry. In addition, it also brings a model calculation of Ref. [24] into an agreement with the observed $K^+\Xi^-$ invariant mass distribution in Ξ photoproduction [66]. The $\Lambda(1890)$ is also required to improve the fit quality in the present model, especially in the energy dependence of the total cross sections of the charged Ξ^- production around $W = 1.9$ GeV. The total cross section data in the charged Ξ^- production seems to indicate a bump structure at around $W = 2.3$ GeV, which is accounted for by the $\Sigma(2250)$ resonance with $J^P = 5/2^-$ and a mass of 2265 MeV in the present model. More accurate data are required before a more definitive answer can be provided for the role of these two resonances. In this regard, the multi-strangeness hyperon production programs using an intense anti-Kaon beam at J-PARC is of particular relevance in providing the much needed higher-precision data for the present reaction.

Apart from the recoil asymmetry, we have also predicted the target-recoil asymmetries for which there are no experimental data currently. In contrast to the recoil polarization — which are small — these observables are quite sizable and may help impose more stringent constraints on the model parameters. In principle, one requires four independent observables as have been considered in this work to model-independently determine the reaction amplitude [55]. Of course, measurements of these spin observables are challenging experimentally by any standard, but one can exploit the self-analyzing nature of the produced hyperon to extract these observables [55, 67]. Of course, for the target-recoil asymmetry measurements, one requires a polarized target in addition to spin measurements of the produced Ξ . The issue of the measurement of the spin of the cascade is already addressed in the previous sentence, as one can exploit the self-analyzing nature of the cascade. The polarized targets are nowadays available at some of the major laboratories worldwide. Combined with the availability of intense beams, measuring these spin observables is no longer out of reach. In fact, various single- and double-polarization observables in photoproduction reactions are currently being measured at the major facilities such as JLab, ELSA, and MAMI, aiming at the so-called complete experiments in order to model-independently determine the photoproduction amplitudes.

There are some controversy about the role of particular resonances among the recent calculations of the $K^- + N \rightarrow K + \Xi$ reaction, in particular, those based on effective Lagrangians as mentioned in the Intro-

duction [50, 51] and now including the present work. The common feature among these calculations, including that based on the Unitarized Chiral Perturbation approach [52], is that some $S = -1$ hyperon resonances seem to be required to reproduce the existing data. To pin down the role of a particular resonance among them requires more precise and complete data, in addition to a more complete theoretical model. Anyway, the present reaction is very suited for studying $S = -1$ hyperon resonances.

Finally, the present work is our first step toward building a more complete reaction theory to help analyze the data and extract the properties of Ξ resonances in future experimental efforts in Ξ baryon spectroscopy. This is a complementary work to that of a model-independent analysis performed recently by the same authors [55] and will also help in analyzing the data to understand the production mechanisms of Ξ baryons.

ACKNOWLEDGMENTS

We are grateful to D. A. Sharov for providing us with the digitized version of the data used in the present work. This work was supported by the National Research Foundation of Korea funded by the Korean Government (Grant No. NRF-2011-220-C00011). The work of Y.O. was also supported in part by the Ministry of Science, ICT, and Future Planning (MSIP) and the National Research Foundation of Korea under Grant No. NRF-2013K1A3A7A06056592 (Center for Korean J-PARC Users). The work of K.N. was also supported in part by the FFE-COSY Grant No. 41788390.

Appendix

In this Appendix, we give the effective Lagrangians and phenomenological dressed baryon propagators from which the s - and u -channel amplitudes M_s and M_u discussed in Sec. II are constructed. We follow Refs. [23, 24, 68–70] and consider not only the spin-1/2 ground state Λ and Σ but also their respective excited states with spin up to 7/2. In the following we use the notations for the iso-doublet fields

$$\begin{aligned} N &= \begin{pmatrix} p \\ n \end{pmatrix}, & \Xi &= \begin{pmatrix} \Xi^0 \\ -\Xi^- \end{pmatrix}, \\ K &= \begin{pmatrix} K^+ \\ K^0 \end{pmatrix}, & K_c &= \begin{pmatrix} \bar{K}^0 \\ -K^- \end{pmatrix}, \end{aligned} \quad (\text{A.1})$$

and for the iso-triplet fields

$$\Sigma = \begin{pmatrix} \Sigma^+ \\ \Sigma^0 \\ \Sigma^- \end{pmatrix}. \quad (\text{A.2})$$

We also introduce the auxiliary operators in Dirac space

$$D_{B'BM}^{1/2(\pm)} \equiv -\Gamma^{(\pm)} \left[\pm i\lambda + \frac{1-\lambda}{m_{B'} \pm m_B} \not{\partial} \right], \quad (\text{A.3a})$$

$$D_\nu^{3/2(\pm)} \equiv \Gamma^{(\mp)} \partial_\nu, \quad (\text{A.3b})$$

$$D_{\mu\nu}^{5/2(\pm)} \equiv -i\Gamma^{(\pm)} \partial_\mu \partial_\nu, \quad (\text{A.3c})$$

$$D_{\mu\nu\rho}^{7/2(\pm)} \equiv -\Gamma^{(\mp)} \partial_\mu \partial_\nu \partial_\rho, \quad (\text{A.3d})$$

where $\Gamma^{(+)} \equiv \gamma_5$ and $\Gamma^{(-)} \equiv 1$. Here, m_B stands for the mass of the baryon B . The parameter λ has been introduced to interpolate between the pseudovector ($\lambda = 0$) and the pseudoscalar ($\lambda = 1$) couplings. Note that in the above equation the order of the subscript indices in $D_{B'BM}^{1/2(\pm)}$ is important, i.e., $D_{B'BM}^{1/2(\pm)} \neq D_{BB'M}^{1/2(\pm)}$.

The effective Lagrangians for spin-1/2 hyperons Λ and Σ (or their resonances) are, then, given by

$$\mathcal{L}_{\Lambda NK}^{1/2(\pm)} = g_{\Lambda NK} \bar{\Lambda} \left\{ D_{\Lambda NK}^{1/2(\pm)} \bar{K} \right\} N + \text{H.c.}, \quad (\text{A.4a})$$

$$\mathcal{L}_{\Sigma NK}^{1/2(\pm)} = g_{\Sigma NK} \bar{\Sigma} \cdot \left\{ D_{\Sigma NK}^{1/2(\pm)} \bar{K} \right\} \tau N + \text{H.c.}, \quad (\text{A.4b})$$

$$\mathcal{L}_{\Xi \Lambda K_c}^{1/2(\pm)} = g_{\Xi \Lambda K_c} \bar{\Xi} \left\{ D_{\Xi \Lambda K_c}^{1/2(\pm)} K_c \right\} \Lambda + \text{H.c.}, \quad (\text{A.4c})$$

$$\mathcal{L}_{\Xi \Sigma K_c}^{1/2(\pm)} = g_{\Xi \Sigma K_c} \bar{\Xi} \tau \left\{ D_{\Xi \Sigma K_c}^{1/2(\pm)} K_c \right\} \cdot \Sigma + \text{H.c.}, \quad (\text{A.4d})$$

where the superscripts \pm refer to the positive (+) and negative (−) relative parity of the baryons. Flavor SU(3) symmetry relates the coupling constants among the members of the octet $J^P = 1/2^+$ ground state baryons and $J^P = 0^+$ pseudoscalar mesons and we have

$$g_{\Lambda NK} = -g_8 \frac{1+2\alpha}{\sqrt{3}}, \quad (\text{A.5a})$$

$$g_{\Sigma NK} = g_8(1-2\alpha), \quad (\text{A.5b})$$

$$g_{\Xi \Lambda K_c} = -g_8 \frac{1-4\alpha}{\sqrt{3}}, \quad (\text{A.5c})$$

$$g_{\Xi \Sigma K_c} = -g_8, \quad (\text{A.5d})$$

where $g_8 = g_{NN\pi} = 13.45$ empirically and the D/F mixing parameter $\alpha = 2/5$ from SU(6) considerations.

For spin-3/2 hyperons, we have

$$\mathcal{L}_{\Lambda NK}^{3/2(\pm)} = \frac{g_{\Lambda NK}}{m_K} \bar{\Lambda}^\nu \left\{ D_\nu^{3/2(\pm)} \bar{K} \right\} N + \text{H.c.}, \quad (\text{A.6a})$$

$$\mathcal{L}_{\Sigma NK}^{3/2(\pm)} = \frac{g_{\Sigma NK}}{m_K} \bar{\Sigma}^\nu \cdot \left\{ D_\nu^{3/2(\pm)} \bar{K} \right\} \tau N + \text{H.c.}, \quad (\text{A.6b})$$

$$\mathcal{L}_{\Xi \Lambda K_c}^{3/2(\pm)} = \frac{g_{\Xi \Lambda K_c}}{m_K} \bar{\Xi} \left\{ D_\nu^{3/2(\pm)} K_c \right\} \Lambda^\nu + \text{H.c.}, \quad (\text{A.6c})$$

$$\mathcal{L}_{\Xi \Sigma K_c}^{3/2(\pm)} = \frac{g_{\Xi \Sigma K_c}}{m_K} \bar{\Xi} \tau \left\{ D_\nu^{3/2(\pm)} K_c \right\} \cdot \Sigma^\nu + \text{H.c.}, \quad (\text{A.6d})$$

where m_K denotes the kaon mass. For spin-5/2 hyperons [24, 71],

$$\mathcal{L}_{\Lambda NK}^{5/2(\pm)} = \frac{g_{\Lambda NK}}{m_K^2} \bar{\Lambda}^{\mu\nu} \left\{ D_{\mu\nu}^{5/2(\pm)} \bar{K} \right\} N + \text{H.c.}, \quad (\text{A.7a})$$

$$\mathcal{L}_{\Sigma NK}^{5/2(\pm)} = \frac{g_{\Sigma NK}}{m_K^2} \bar{\Sigma}^{\mu\nu} \cdot \left\{ D_{\mu\nu}^{5/2(\pm)} \bar{K} \right\} \tau N + \text{H.c.}, \quad (\text{A.7b})$$

$$\mathcal{L}_{\Xi \Lambda K_c}^{5/2(\pm)} = \frac{g_{\Xi \Lambda K_c}}{m_K^2} \bar{\Xi} \left\{ D_{\mu\nu}^{5/2(\pm)} K_c \right\} \Lambda^{\mu\nu} + \text{H.c.}, \quad (\text{A.7c})$$

$$\mathcal{L}_{\Xi \Sigma K_c}^{5/2(\pm)} = \frac{g_{\Xi \Sigma K_c}}{m_K^2} \bar{\Xi} \tau \left\{ D_{\mu\nu}^{5/2(\pm)} K_c \right\} \cdot \Sigma^{\mu\nu} + \text{H.c.}. \quad (\text{A.7d})$$

And for spin-7/2 hyperons we have [24, 71]

$$\mathcal{L}_{\Lambda NK}^{7/2(\pm)} = \frac{g_{\Lambda NK}}{m_K^3} \bar{\Lambda}^{\mu\nu\rho} \left\{ D_{\mu\nu\rho}^{7/2(\pm)} \bar{K} \right\} N + \text{H.c.}, \quad (\text{A.8a})$$

$$\mathcal{L}_{\Sigma NK}^{7/2(\pm)} = \frac{g_{\Sigma NK}}{m_K^3} \bar{\Sigma}^{\mu\nu\rho} \cdot \left\{ D_{\mu\nu\rho}^{7/2(\pm)} \bar{K} \right\} \tau N + \text{H.c.}, \quad (\text{A.8b})$$

$$\mathcal{L}_{\Xi \Lambda K_c}^{7/2(\pm)} = \frac{g_{\Xi \Lambda K_c}}{m_K^3} \bar{\Xi} \left\{ D_{\mu\nu\rho}^{7/2(\pm)} K_c \right\} \Lambda^{\mu\nu\rho} + \text{H.c.}, \quad (\text{A.8c})$$

$$\mathcal{L}_{\Xi \Sigma K_c}^{7/2(\pm)} = \frac{g_{\Xi \Sigma K_c}}{m_K^3} \bar{\Xi} \tau \left\{ D_{\mu\nu\rho}^{7/2(\pm)} K_c \right\} \cdot \Sigma^{\mu\nu\rho} + \text{H.c.}. \quad (\text{A.8d})$$

The coupling constants in the above Lagrangians corresponding to Λ and Σ resonances are free parameters adjusted to reproduce the existing data. For those resonances considered in the present work, they are given in Table III.

The MBr vertices $\hat{\Gamma}_{MBr}^\dagger(\hat{\Gamma}_{MBr})$ in Eq. (11) are obtained from the above Lagrangians. In addition, each MBr vertex is multiplied by an off-shell form factor given by

$$f(p_r^2, m_r, \Lambda_r) = \left(\frac{n\Lambda_r^4}{n\Lambda_r^4 + (p_r^2 - m_r^2)^2} \right)^n, \quad (\text{A.9})$$

where p_r^2 and m_r are the square of the 4-momentum and mass of the exchanged hyperon, respectively. The cutoff parameter Λ_r is chosen to have a common value $\Lambda_r \equiv \Lambda = 900$ MeV for all the MBr vertices in order to keep the number of free parameters to a minimum. Also, we choose $n = 1$.

For the propagators of the dressed hyperons in Eq. (11), we could in principle adopt the forms used in our previous work [24, 68–70]. However, in view of the limited amount of currently available data for the present reaction and the rather poor quality of these data, here we adopt the simpler forms as given in the following. For a spin-1/2 baryon propagator, we use

$$\hat{S}_r^{1/2}(p_r) = \frac{1}{\not{p}_r - m_r + i\frac{\Gamma_r}{2}}, \quad (\text{A.10})$$

where Γ_r is the baryon width assumed to be constant, independent of energy. For a stable (ground state) baryon, $\Gamma_r \rightarrow \epsilon$ with ϵ being positive infinitesimal.

For spin-3/2, the dressed propagator reads in a schematic matrix notation

$$\hat{S}_r^{3/2}(p_r) = \frac{1}{\not{p}_r - m_r + i\frac{\Gamma_r}{2}} \Delta, \quad (\text{A.11})$$

where Δ is the Rarita-Schwinger tensor given by

$$\Delta \equiv \Delta^{\mu\nu} = -g^{\mu\nu} + \frac{1}{3}\gamma^\mu\gamma^\nu + \frac{2p^\mu p^\nu}{3m_r^2} + \frac{\gamma^\mu p^\nu - p^\mu \gamma^\nu}{3m_r}. \quad (\text{A.12})$$

Similarly, the propagator for a spin-5/2 resonance is given by

$$\hat{S}_r^{5/2}(p_r) = \frac{1}{\not{p}_r - m_r + i\frac{\Gamma_r}{2}}\Delta, \quad (\text{A.13})$$

where [71]

$$\begin{aligned} \Delta &\equiv \Delta_{\alpha_1\alpha_2}^{\beta_1\beta_2} \\ &= \frac{1}{2} \left(\bar{g}_{\alpha_1}^{\beta_1} \bar{g}_{\alpha_2}^{\beta_2} + \bar{g}_{\alpha_1}^{\beta_2} \bar{g}_{\alpha_2}^{\beta_1} \right) - \frac{1}{5} \bar{g}_{\alpha_1\alpha_2} \bar{g}^{\beta_1\beta_2} \\ &\quad - \frac{1}{10} \left(\bar{\gamma}_{\alpha_1} \bar{\gamma}^{\beta_1} \bar{g}_{\alpha_2}^{\beta_2} + \bar{\gamma}_{\alpha_1} \bar{\gamma}^{\beta_2} \bar{g}_{\alpha_2}^{\beta_1} + \bar{\gamma}_{\alpha_2} \bar{\gamma}^{\beta_1} \bar{g}_{\alpha_1}^{\beta_2} \right. \\ &\quad \left. + \bar{\gamma}_{\alpha_2} \bar{\gamma}^{\beta_2} \bar{g}_{\alpha_1}^{\beta_1} \right) \end{aligned} \quad (\text{A.14})$$

with

$$\bar{g}^{\mu\nu} \equiv g^{\mu\nu} - \frac{p^\mu p^\nu}{m_r^2}, \quad \bar{\gamma}^\mu \equiv \gamma^\mu - \frac{p^\mu \not{p}}{m_r^2}. \quad (\text{A.15})$$

The propagator for a spin-7/2 resonance is given by

$$\hat{S}_r^{7/2}(p_r) = \frac{1}{\not{p}_r - m_r + i\frac{\Gamma_r}{2}}\Delta, \quad (\text{A.16})$$

where [71]

$$\begin{aligned} \Delta &\equiv \Delta_{\alpha_1\alpha_2\alpha_3}^{\beta_1\beta_2\beta_3} \\ &= \frac{1}{36} \sum_{P(\alpha), P(\beta)} \left\{ \bar{g}_{\alpha_1}^{\beta_1} \bar{g}_{\alpha_2}^{\beta_2} \bar{g}_{\alpha_3}^{\beta_3} - \frac{3}{7} \bar{g}_{\alpha_1}^{\beta_1} \bar{g}_{\alpha_2\alpha_3} \bar{g}^{\beta_2\beta_3} \right. \\ &\quad \left. - \frac{3}{7} \bar{\gamma}_{\alpha_1} \bar{\gamma}^{\beta_1} \bar{g}_{\alpha_2}^{\beta_2} \bar{g}_{\alpha_3}^{\beta_3} + \frac{3}{35} \bar{\gamma}_{\alpha_1} \bar{\gamma}^{\beta_1} \bar{g}_{\alpha_2\alpha_3} \bar{g}^{\beta_2\beta_3} \right\}, \end{aligned} \quad (\text{A.17})$$

and the summation runs over all possible permutations of $\{\alpha_1, \alpha_2, \alpha_3\}$ and of $\{\beta_1, \beta_2, \beta_3\}$.

-
- [1] R. G. Edwards, N. Mathur, D. G. Richards, and S. J. Wallace (Hadron Spectrum Collaboration), Flavor structure of the excited baryon spectra from lattice QCD, *Phys. Rev. D* **87**, 054506 (2013).
- [2] G. P. Engel, C. B. Lang, D. Mohler, and A. Schäfer (BGR [Bern-Graz-Regensburg] Collaboration), QCD with two light dynamical chirally improved quarks: Baryons, *Phys. Rev. D* **87**, 074504 (2013).
- [3] D. J. Wilson, I. C. Cloet, L. Chang, and C. D. Roberts, Nucleon and Roper electromagnetic elastic and transition form factors, *Phys. Rev. C* **85**, 025205 (2012).
- [4] S. Capstick and W. Roberts, Quark models of baryon masses and decays, *Prog. Part. Nucl. Phys.* **45**, S241 (2000).
- [5] M. Röniger and B. C. Metsch, Effects of a spin-flavour dependent interaction on the baryon mass spectrum, *Eur. Phys. J. A* **47**, 162 (2011).
- [6] Y. Oh, Ξ and Ω baryons in the Skyrme model, *Phys. Rev. D* **75**, 074002 (2007).
- [7] E. Oset and A. Ramos, Dynamically generated resonances from the vector octet-baryon octet interaction, *Eur. Phys. J. A* **44**, 445 (2010).
- [8] M. Mai, P. C. Bruns, and U.-G. Meissner, Pion photoproduction off the proton in a gauge-invariant chiral unitary framework, *Phys. Rev. D* **86**, 094033 (2012).
- [9] R. Arndt, W. Briscoe, I. Strakovsky, and R. Workman, Partial-wave analysis and baryon spectroscopy, *Eur. Phys. J. A* **35**, 311 (2008).
- [10] A. V. Anisovich, R. Beck, E. Klempt, V. A. Nikonov, A. V. Sarantsev, and U. Thoma, Properties of baryon resonances from a multichannel partial wave analysis, *Eur. Phys. J. A* **48**, 15 (2012).
- [11] G. Y. Chen, S. S. Kamalov, S. N. Yang, D. Drechsel, and L. Tiator, Nucleon resonances in πN scattering up to energies $\sqrt{s} \leq 2.0$ GeV, *Phys. Rev. C* **76**, 035206 (2007).
- [12] L. Tiator, S. S. Kamalov, S. Ceci, G. Y. Chen, D. Drechsel, A. Svarc, and S. N. Yang, Singularity structure of the πN scattering amplitude in a meson-exchange model up to energies $W \leq 2.0$ GeV, *Phys. Rev. C* **82**, 055203 (2010).
- [13] V. Shklyar, H. Lenske, and U. Mosel, η -meson production in the resonance energy region, *Phys. Rev. C* **87**, 015201 (2013).
- [14] A. Matsuyama, T. Sato, and T.-S. H. Lee, Dynamical coupled-channel model of meson production reactions in the nucleon resonance region, *Phys. Rep.* **439**, 193 (2007).
- [15] H. Kamano, S. X. Nakamura, T.-S. H. Lee, and T. Sato, Extraction of P_{11} resonances from πN data, *Phys. Rev. C* **81**, 065207 (2010).
- [16] D. Rönchen, M. Döring, F. Huang, H. Haberzettl, J. Haidenbauer, C. Hanhart, S. Krewald, U. G. Meißner, and K. Nakayama, Coupled-channel dynamics in the reactions $\pi N \rightarrow \pi N$, ηN , $K\Lambda$, $K\Sigma$, *Eur. Phys. J. A* **49**, 44 (2013).
- [17] K. A. Olive *et al.* (Particle Data Group), Review of particle physics, *Chin. Phys. C* **38**, 090001 (2014).
- [18] E. Klempt and J.-M. Richard, Baryon spectroscopy, *Rev. Mod. Phys.* **82**, 1095 (2010).
- [19] L. Guo *et al.* (CLAS Collaboration), Cascade production in the reactions $\gamma p \rightarrow K^+ K^+(X)$ and $\gamma p \rightarrow K^+ K^+ \pi^-(X)$, *Phys. Rev. C* **76**, 025208 (2007).
- [20] V. Flaminio, W. G. Moorhead, D. R. O. Morrison, and N. Rivoire (High-Energy Reactions Analysis Group), CERN Report No. CERN-HERA-83-02.
- [21] H.-Y. Ryu, A. Hosaka, H. Haberzettl, H.-C. Kim, K. Nakayama, and Y. Oh, Hadronic description for Omega baryon photoproduction, *PoS Hadron2013*, 140

- (2013), [arXiv:1401.3804].
- [22] A. Afanasev *et al.* (The Very Strange Collaboration), Photoproduction of the very strangest baryons on a proton target in CLAS12, JLab. Report No. JLAB-PR-12-008.
 - [23] K. Nakayama, Y. Oh, and H. Haberzettl, Photoproduction of Ξ off nucleons, *Phys. Rev. C* **74**, 035205 (2006).
 - [24] J. K. S. Man, Y. Oh, and K. Nakayama, Role of high-spin hyperon resonances in the reaction of $\gamma p \rightarrow K^+ K^+ \Xi^-$, *Phys. Rev. C* **83**, 055201 (2011).
 - [25] J. K. Ahn, Production of Ξ^* resonances in the $K^- p$ interaction at J-PARC, *J. Korean Phys. Soc.* **49**, 2276 (2006).
 - [26] H. Takahashi, $S = -3$ physics at J-PARC, *Nucl. Phys. A* **914**, 553 (2013).
 - [27] W. Erni *et al.* (The PANDA Collaboration), Physics performance report for PANDA: Strong interaction studies with antiprotons, arXiv:0903.3905.
 - [28] G. M. Pjerrou, D. J. Prowse, P. Schlein, W. E. Slater, D. H. Stork, and H. K. Ticho, Resonance in the $(\Xi\pi)$ System at 1.53 GeV, *Phys. Rev. Lett.* **9**, 114 (1962).
 - [29] D. D. Carmony, G. M. Pjerrou, P. E. Schlein, W. E. Slater, D. H. Stork, and H. K. Ticho, Properties of Ξ hyperons, *Phys. Rev. Lett.* **12**, 482 (1964).
 - [30] J. P. Berge, P. Eberhard, J. R. Hubbard, D. W. Merrill, J. Button-Shafer, F. T. Solmitz, and M. L. Stevenson, Some properties of Ξ^- and Ξ^0 hyperons produced in $K^- p$ interactions between 1.05 and 1.7 BeV/c, *Phys. Rev.* **147**, 945 (1966).
 - [31] M. Haque *et al.* (Birmingham-Glasgow-London(I.C.)-Oxford-Rutherford Collaboration), Reactions $K^- p \rightarrow \text{Hyperon} + \text{Meson}$ at 3.5 GeV/c, *Phys. Rev.* **152**, 1148 (1966).
 - [32] G. W. London, R. R. Rau, N. P. Samios, S. S. Yamamoto, M. Goldberg, S. Lichtman, M. Prime, and J. Leitner, $K^- p$ interaction at 2.24 BeV/c, *Phys. Rev.* **143**, 1034 (1966).
 - [33] T. G. Trippe and P. E. Schlein, Partial-wave analysis of $K^- p \rightarrow \Xi^- K^+$ at 2 GeV/c, *Phys. Rev.* **158**, 1334 (1967).
 - [34] W. P. Trower, J. R. Ficenec, R. I. Hulsizer, J. Lathrop, J. N. Snyder, and W. P. Swanson, Some two-body final states of $K^- p$ interactions at 1.33 GeV/c, *Phys. Rev.* **170**, 1207 (1968).
 - [35] D. W. Merrill and J. Button-Shafer, Properties of the Ξ^- and the $\Xi(1817)$ from $K^- p$ Interactions above 1.7 BeV/c, *Phys. Rev.* **167**, 1202 (1968).
 - [36] G. Burgun *et al.*, Resonance formation in the reactions $K^- p \rightarrow K^+ \Xi^-$ and $K^- p \rightarrow K^0 \Xi^0$ in the mass region from 1915 to 2168 MeV, *Nucl. Phys. B* **8**, 447 (1968).
 - [37] P. M. Dauber, J. P. Berge, J. R. Hubbard, D. W. Merrill, and R. A. Muller, Production and decay of cascade hyperons, *Phys. Rev.* **179**, 1262 (1969).
 - [38] J. C. Scheuer *et al.* (S.A.B.R.E. Collaboration), Experimental study of two-body and quasi-two-body reactions in $K^- n$ interactions at 3 GeV/c, *Nucl. Phys. B* **33**, 61 (1971).
 - [39] A. de Bellefon *et al.*, Channel cross-sections of $K^- p$ reactions from 1.26 to 1.84 GeV/c, *Nuovo Cim. A* **7**, 567 (1972).
 - [40] J. R. Carlson, H. F. Davis, D. E. Jauch, N. D. Sossong, and R. Ellsworth, Measurement of neutral cascade production from, *Phys. Rev. D* **7**, 2533 (1973).
 - [41] R. Rader *et al.*, The reaction $K^- p \rightarrow \Lambda \eta$ from 0.80 to 1.84 GeV/c, *Nuovo Cim. A* **16**, 178 (1973).
 - [42] J. Griselin *et al.*, $K^- p$ cross sections between 1.1 and 1.4 GeV/c, *Nucl. Phys. B* **93**, 189 (1975).
 - [43] E. Briefel *et al.*, Search for Ξ^* production in $K^- p$ reactions at 2.87 GeV/c, *Phys. Rev. D* **16**, 2706 (1977).
 - [44] O. Dumbrajs, R. Koch, H. Pilkuhn, G. C. Oades, H. Behrens, J. J. de Swart, and P. Kroll, Compilation of coupling constants and low-energy parameters: 1982-Edition, *Nucl. Phys. B* **216**, 277 (1983).
 - [45] M. E. Ebel and P. B. James, Peripheral model for Ξ^- associated productions, *Phys. Rev.* **153**, 1694 (1967).
 - [46] P. B. James, Baryon exchange in Ξ production processes, *Phys. Rev.* **158**, 1617 (1967).
 - [47] B. K. Agarwal, C. P. Singh, K. J. Narain, and A. B. Saxena, $K^- p \rightarrow K^+ \Xi^-$ process in the two-meson-exchange peripheral model, *J. Phys. A* **4**, L52 (1971).
 - [48] K. L. Mir and J. K. Storrow, Hyperon-exchange reactions at high energies. III. Backward $KN \rightarrow \Xi K$ scattering, *J. Phys. G* **8**, 465 (1982).
 - [49] C. B. Dover and A. Gal, Ξ hypernuclei, *Ann. Phys. (N.Y.)* **146**, 309 (1983).
 - [50] D. A. Sharov, V. L. Korotkikh, and D. E. Lansko, Phenomenological model for the $\bar{K}N \rightarrow K\Xi$ reaction, *Eur. Phys. J. A* **47**, 109 (2011).
 - [51] R. Shyam, O. Scholten, and A. W. Thomas, Production of a Cascade hyperon in the K^- -proton interaction, *Phys. Rev. C* **84**, 042201 (2011).
 - [52] V. K. Magas, A. Feijoo, and A. Ramos, The $K^- N \rightarrow K\Xi$ reaction in coupled channel chiral models up to next-to-leading order, *AIP Conf. Proc.* **1606**, 208 (2014).
 - [53] H. Kamano, S. X. Nakamura, T.-S. H. Lee, and T. Sato, Dynamical coupled-channels model of $K^- p$ reactions: Determination of partial-wave amplitudes, *Phys. Rev. C* **90**, 065204 (2014).
 - [54] K. Nakayama, Y. Oh, and H. Haberzettl, Model-independent determination of the parity of Ξ hyperons, *Phys. Rev. C* **85**, 042201(R) (2012).
 - [55] B. Jackson, Y. Oh, H. Haberzettl, and K. Nakayama, Model-independent aspects of the reaction $\bar{K} + N \rightarrow K + \Xi$, *Phys. Rev. C* **89**, 025206 (2014).
 - [56] Y. Yamamoto, T. Motoba, T. Fukuda, M. Takahashi, and K. Ikeda, Formation and transition of strangeness $S = -2$ nuclear systems, *Prog. Theor. Phys. Suppl.* **117**, 281 (1994).
 - [57] S. Tadokoro, H. Kobayashi, and Y. Akaishi, Ξ^- -hypernuclear states in heavy nuclei, *Phys. Rev. C* **51**, 2656 (1995).
 - [58] M. Kohn and S. Hashimoto, Ξ -nucleus potential and (K^-, K^+) inclusive spectrum at Ξ^- production threshold region, *Prog. Theor. Phys.* **123**, 157 (2010).
 - [59] K. Nakayama and W. G. Love, Spin structure of spin-1/2 baryon and spinless meson production amplitudes in photonic and hadronic reactions, *Phys. Rev. C* **72**, 034603 (2005).
 - [60] M. Döring and K. Nakayama, On the cross section ratio σ_n/σ_p in η photoproduction, *Phys. Lett. B* **683**, 145 (2010).
 - [61] A. Ramos and E. Oset, The role of vector-baryon channels and resonances in the $\gamma p \rightarrow K^0 \Sigma^+$ and $\gamma n \rightarrow K^0 \Sigma^0$ reactions near the $K^* \Lambda$ threshold, *Phys. Lett. B* **727**, 287 (2013).
 - [62] H.-Y. Ryu, A. I. Titov, A. Hosaka, and H.-C. Kim, ϕ photoproduction with coupled-channel effects, *Prog. Theor. Exp. Phys.* **2014**, 023D03 (2014).

- [63] H. Ryu, A. Hosaka, H.-C. Kim, and A. I. Titov, Photo-production of phi meson near the threshold, *Int. J. Mod. Phys. Conf. Ser.* **26**, 1460055 (2014).
- [64] D. Plümper, J. Flender, and M. F. Gari, Nucleon-nucleon interaction from meson exchange and nucleonic structure, *Phys. Rev. C* **49**, 2370 (1994).
- [65] R. Shyam and O. Scholten, Photoproduction of η mesons within a coupled-channels K -matrix approach, *Phys. Rev. C* **78**, 065201 (2008).
- [66] L. Guo *et al.* (CLAS Collaboration), Cascade production in the reactions $\gamma p \rightarrow K^+ K^+(X)$ and $\gamma p \rightarrow K^+ K^+ \pi^-(X)$, *Phys. Rev. C* **76**, 025208 (2007).
- [67] K. Moriya *et al.* (CLAS Collaboration), Spin and parity measurement of the $\Lambda(1405)$ baryon, *Phys. Rev. Lett.* **112**, 082004 (2014).
- [68] K. Nakayama and H. Haberzettl, Consistent analysis of the reactions $\gamma p \rightarrow p\eta'$ and $pp \rightarrow pp\eta'$, *Phys. Rev. C* **69**, 065212 (2004).
- [69] K. Nakayama and H. Haberzettl, Analyzing η' photoproduction data on the proton at energies of 1.5–2.3 GeV, *Phys. Rev. C* **73**, 045211 (2006).
- [70] K. Nakayama, Y. Oh, and H. Haberzettl, Combined analysis of η meson hadro- and photo-production off nucleons, *J. Korean Phys. Soc.* **59**, 224 (2011).
- [71] S.-J. Chang, Lagrange formulation for systems with higher spin, *Phys. Rev.* **161**, 1308 (1967).